OAK RIDGE
NATIONAL LABORATORY

MANAGED BY UT-BATTELLE
FOR THE DEPARTMENT OF ENERGY

ORNL/TM-2009/138

SUMMARY OF PRIOR WORK ON JOINING OF OXIDE DISPERSION-STRENGTHENED ALLOYS

May 2009

US-UK Collaboration in Fossil Energy Advanced Materials Program
October 2004 to March 2009

Task 8: Oxide Dispersion-Strengthened Alloys

I. G. Wright,[a] G. Tatlock,[b] H. Al-Badairy,[b] and C-L. Chen[b]
[a]Oak Ridge National Laboratory
[b]University of Liverpool

UT-BATTELLE

ORNL/TM-2008/138

Materials Science and Technology Division

Summary of Prior Work on Joining of Oxide Dispersion-Strengthened Alloys

US-UK Collaboration in Fossil Energy Advanced Materials Program
October 2004 to March 2009

Task 8: Oxide Dispersion-Strengthened Alloys

I. G. Wright,[a] G. Tatlock,[b] H. Al-Badairy,[b] and C-L. Chen[b]
[a]Oak Ridge National Laboratory
[b]University of Liverpool

Date Published: May 2009

Prepared for the
U.S. Department of Energy
Deputy Director for Fossil Energy
AA 15 10 10 0

Prepared by
OAK RIDGE NATIONAL LABORATORY
Oak Ridge, Tennessee 37831-6285
managed by
UT-Battelle, LLC
for the
U.S. DEPARTMENT OF ENERGY
under contract DE-AC05-00OR22725

CONTENTS

Page

LIST OF TABLES

LIST OF FIGURES

EXECUTIVE SUMMARY

There is a range of joining techniques available for use with ODS alloys, but care should be exercised in matching the technique to the final duty requirements of the joint. The goal for joining ODS alloys is a joint with no local disruption of the distribution of the oxide dispersion, and no significant change in the size and orientation of the alloy microstructure. Not surprisingly, the fusion welding processes typically employed with wrought alloys produce the least satisfactory results with ODS alloys, but some versions, such as fusion spot welding, and the laser and electron-beam welding technologies, have demonstrated potential for producing sound joints. Welds made using solid-state spot welding reportedly have exhibited parent metal properties. Thus, it is possible to employ processes that result in significant disruption of the alloy microstructure, as long as the processing parameters are adjustment to minimize the extent of or influence of the changes in the alloy microstructure. Selection among these joining approaches largely depends on the particular application and component configuration, and an understanding of the relationships among processing, alloy microstructure, and final properties is key. Recent developments have resulted in friction welding evolving to be a prime method for joining ODS sheet products, and variants of brazing/diffusion bonding have shown excellent promise for use with tubes and pipes. The techniques that come closest to the goal defined above involve solid-state diffusion bonding and, in particular, it has been found that secondary recrystallization of joints made by pulsed plasma-assisted diffusion can produce the desired, continuous, large alloy grain structure through the joint. Such joints have exhibited creep rupture failure at >82% of the load needed to fail the monolithic parent alloy at 1000°C.

1. OBJECTIVES

The goal of this report is to collect, analyse, and compile results from joining trials with oxide dispersion-strengthened (ODS) alloys reported in the literature to provide a comprehensive documentation of the techniques, procedures, and availability of joining methods available for use with ODS alloys. Where available, details of the methodologies used, and comments on the joints produced (especially microstructures and mechanical properties) have been reproduced. It is intended that this report be supplemented by results from contemporary projects in the area, as information becomes available.

2. BACKGROUND

There have been numerous efforts over the past 35 years by research groups interested in the use of ODS alloys to provide a solution to an otherwise difficult problem in materials selection in a variety of high-temperature applications. These efforts experienced mixed success, but in many cases a workable solution to joining these alloys was found and used. Unfortunately, these instances of success were not widely publicised (possibly because of relatively poor interactions among the nuclear, fossil, and gas turbine communities interested in these alloys), so that the 'discovery' that conventional fusion methods are not appropriate for ODS alloys has been repeated many times, leading to the oft-repeated truism that ODS alloys are not joinable. This report results from a desire to develop a repository of the background to the various systematic attempts that have been made to join ODS alloys, so that future efforts can be built on a rational understanding of the reasons for the failures and successes of the various joining approaches that have been investigated in the past.

Unlike other summaries of joining of ODS alloys (see, for instance, Ref. 1) the aim of this report is to include, where available, details of the intended applications for ODS alloys and the methodologies used to join the various forms of material, together with comments on issues encountered, and evaluation of the joints produced. The inclusion of microstructures was considered to be sufficiently valuable that where micrographs were available in the original reports, they have been included even when of a quality that normally would not be considered acceptable for publication. All reported mechanical property data have been included. The compositions of the ODS alloys of interest are summarized in Table 1, while actual compositions, where available, are presented in Table 2 (in at%) to indicate the levels of minor additions and impurities. While the original intent of this report was to provide a starting point for recent efforts to advance the development and application of ODS alloys [see, for instance, Ref. 2-4], a goal is also for it to be supplemented by results from contemporary projects in the area, as information becomes available. Ultimately, it is hoped that the availability of a compilation of such information will provide a rational basis for selecting the joining method most appropriate for a given application of ODS alloys.

Table 1. Nominal compositions of ODS alloys (wt %)

Alloy	Source	Fe	Ni	Cr	Al	Ti	Mo	C	Dispersion
ODM331	Dour Metal	Bal		13	3	0.6	1.5		0.5 Y_2O_3
ODM751	Dour Metal	Bal		16.5	4.5	0.6	1.5		0.5 Y_2O_3
Fe-13Cr	DT2906			13		2.9	1.5		1.8 TiO_2
Fe-13Cr	DT2203Y05			13		2.2	1.5		0.9 TiO_2; 0.5 Y_2O_3
Incoloy MA957	INCO Int'l.	Bal	0.13	14	0.1	1	0.3	0.01	0.25 Y_2O_3
Incoloy MA956	INCO Int'l.	Bal	0.5[a]	20	4.5	0.5	—	0.1[a]	0.5 Y_2O_3
Incoloy MA956HT	INCO Int'l.	Bal		21.6	5.9	0.4	—		Y_2O_3
PM2000	Plansee	Bal		20	5.5	0.5	—		0.5 Y_2O_3
PM2010	Plansee	Bal		20	5.5	0.5	—		1.0 Y_2O_3
ODS Fe_3Al	ORNL	Bal		2.2	15.9	—	—		Y_2O_3
TDNi	Fansteel	—	Bal	—	—	—	—	—	2 ThO_2
TDNiCr	Fansteel	—	Bal	20	—	—	—	—	2 ThO_2
Inconel MA754	INCO Int'l.	1.0	Bal	20	0.3	0.5	—	0.05	0.6 Y_2O_3
Inconel MA758	INCO Int'l.	1.0	Bal	30	0.3	0.5	—	0.05	0.6 Y_2O_3
Inconel MA760[b]	INCO Int'l.	—	Bal	20	6	—	2	0.05	0.95 Y_2O_3
Inconel MA6000[c]	INCO Int'l.	—	Bal	15	4.5	2.5	2	0.05	1.1 Y_2O_3
PM3030[d]	Plansee	—	Bal	17	6	—	2		1.1 Y_2O_3

[a] max
[b] *also*: 3.5 W, 0.01 B, 0.15 Zr wt %
[c] *also*: 4 W, 2 Ta, 0.01 B, 0.15 Zr wt %
[d] *also*: 3.5 W, 2 Ta wt %

Table 2. Actual compositions of ODS alloys (at. %)

Alloy	Fe	Ni	Cr	Al	Ti	Mo	C	O	Mn	Si	P	N	S	Y	Source
ODM331	Bal	0	13.2	7	0.711	0.815	0.044	1.177	0.058	0.076	—	0.088	—	0.22	ORNL
ODM751	Bal	0	16.4	10	0.61	0.82	0.035	1.58	0.05	0.11	0.01	0.09	0.008	0.24	ORNL
MA957	Bal	0	14.7	0	1.204	0.008	0.046	0.755	0.11	0.078	—	—	0.0103	0.14	[ref. 10]
MA956	Bal	0	20.1	9	0.40	0	0.0635	0.649	0.08	0.13	0.013	0.061	0	0.24	ORNL
MA956HT	Bal	0	21.5	11	0.43	0.01	0.129	0.689	0.06	0.09	—	0.106	0	0.22	ORNL
PM2000	Bal	0	20	11	0.44	0	0.0345	0.743	0.04	0.04	0	0	0	0.233	ORNL
ODS Fe_3Al	Bal	0	2.13	27	0	—	0.158	0.616	0.026	0.051	0.012	0.35	0.003	0.209	ORNL
MA754	0.39	Bal	21.4	1	0.67	0.53	0.23	1.514	—	—	—	—	0.0018	0.36	INCO
MA758	0.4	Bal	33.2	1	0.57	0	0.23	0.99	0	0.12	0	0.68	0	0.28	INCO

3. DESCRIPTION OF AVAILABLE JOINING PROCESSES AND EXPERIENCE WITH ODS ALLOYS

Table 3 lists the joining processes for which some level of documentation has been found, and Tables 1 and 2 list the chemical compositions of the alloys involved in the joining trials described. While relatively few projects have reported details of the resulting microstructures or mechanical properties, joints made by the following processes were successfully used in practice: explosive bonding; transient liquid-phase bonding; laser welding; and brazing.

Table 3. Summary of joining processes used for ODS alloys

Report Section	Joining process	Application	Reference
5.1	Fusion welding	Rods; bar; tubes	5-13
5.2	Laser welding	Sheet; honeycomb structures	12-15
5.3	Electron beam welding	Sheet	7, 13-14
6	Brazing	(a) Tube-corner block joints (HiPPS project) (b) Tube-manifold/end cap joints (COST 522)	7, 13, 16-25
7.3	Flash butt/resistance welding	Fuel pin end cap-tube joints; tubes	10, 26-31
7.4	Torsional resistance forge welding	Fuel pin end cap-tube joints; tubes	31, 32
7.5	Resistance spot welding	Sheet	7
7.6	Resistant seam welding	Sheet	7
8	Electro-spark discharge	Work in progress (EWI-DOE/ STTR project)	26, 34
9	Explosive bonding	Tube/safe ends (COST 501)	7, 30, 35-38
10	Friction welding		
10	Inertia-driven friction welding	Flanges/end caps to tubes	3, 30, 39
10	Friction stir welding	Sheet (combustor cans)	29, 40-49
11	Pulsed magnetic welding	Fuel pin end cap-tube joints; tube-tube	10, 30, 32, 50
12	Diffusion bonding	Sheet; tubes	7, 14, 31, 42, 51
13	Transient liquid-phase bonding	Butt joints in tubes	31, 52-61
14	Pulsed plasma-assisted diffusion bonding	Butt joints in tubes; seal welds	2, 62-65
15	Mechanical joints	Bolting; threaded joints	7, 22

4. FUSION WELDING

4.1 PROCESS DESCRIPTION

The fundamentals of fusion welding have been well summarized elsewhere.[5] Essentially, fusion welding involves a heat source, and may involve the use of a filler material such as a consumable electrode or a wire fed into the weld pool. These processes also use a protective layer between the ambient environment and the molten metal, either in the form of gas shielding or a flux, which melts to give a viscous slag on the weld metal that eventually solidifies (and can be removed after joining). There are several different types of fusion welding processes that can be used, with variations in heat source, type of filler material, and local environment. Table 4 lists some key features for the different procedures and the typical characteristics of the techniques.

Table 4. Summary of fusion welding processes

Process	Cost	Weld cleanliness	HAZ width (mm)	Automation	Plate thickness (mm)	Characteristics
Tungsten inert gas (TIG)	low/med	good	2-3	medium	all (multi-pass)	used for similar applications as MIG/ longer production runs
Manual metal arc (MMA)	low	poor	5-6	none	all (multi-pass)	
Submerged arc welding (SAW)	medium	poor	7-10	very high	all (multi-pass)	used only horizontally; for high production runs
Metal inert gas (MIG)	low/med	acceptable	3-4	medium	all (multi-pass)	used for thinner sections than SAW
Laser	very high	very good	< 0.5[a]	very high	up to 30	used for higher-specification welds; low distortion; requires good fit-up; no filler wires
Electron beam	very high	very good	< 0.5[a]	low	up to 250	requires a vacuum; can be used for welding a range of alloys and reactive metals; low distortion; requires good fit-up; no filler wires

Fusion welding using heat sources other than electric arcs is possible. In particular, laser and electron beams offer higher energy densities than are possible with electric arcs, and this feature provides advantages such as eliminating the need to use filler metals, clean joints, and the production of very narrow heat-affected zones.

4.2 APPLICATION TO ODS ALLOYS

Fusion welding of ODS alloys tends to result in disruption of the dispersion of oxide particles in the fusion zone, since the dispersed oxide particles (typically Y_2O_3) are not wetted by the molten alloy and tend to float into the melt pool. Agglomeration of the dispersoid particles can lead to the formation of inclusions in the fusion zone.[6,7,8] Also, fusion welding tends to significantly change the alloy microstructure necessary for high-temperature strength, so that in the fusion zone all benefits of thermomechanical processing and texture are effectively negated. Fusion also may release entrapped/adsorbed gases, which can result in porosity in the weld or heat-affected zone. Such void formation especially is a problem with Al-containing (alumina scale-forming) ODS alloys.

If fusion welding is practiced, disruption of the dispersoid distribution can be minimized by the careful application of techniques such as MIG or TIG, with preheating, minimum inter-pass temperatures, and a post-weld heat treatment to prevent cracking.[9] If it is impossible to avoid highly-restrained joint designs, post-weld stress relieving should be carried out as soon as practicable to avoid delayed stress cracking. A treatment of 2 h at 1100°C in air followed by air cooling is suggested.[10] The same cycle may serve as a pre-oxidation treatment provided the surface is cleaned of lubricants and other contaminants.

Special Metals Corp.[6] reported relatively low-strength joints from conventional TIG welding, but that this process is acceptable for positioning and fillet-type welds. Suitable filler wires are Inconel filler metal 82 for dissimilar metal joints to Ni-base alloys, and matching composition wires for welding to austenitic stainless steels. For joining the alloy to itself, a Fe-Cr-Al wire is recommended where high-temperature oxidation resistance is required in the weld.

Others also have reported reduced creep strength in a TIG-welded Ni-based ODS alloy (MA754) due to agglomeration of the dispersoid and discontinuity in the microstructure;[11] TIG-welded MA956, using a near-matching FeCrAl filler alloy, reportedly retained only 20-40% of the high-temperature stress rupture strength of the parent alloy.[12] These changes in the microstructure and local composition in the welded zone resulted in reduction of the hardness, and were thought likely to lead to susceptibility to corrosion attack. While GTA welding has been used to join Ni-based ODS alloys (TD-NiCr; MA758) using Ni-based alloys with at least 30% Cr as filler metals, the usual problems of dispersoid agglomeration and microstructure disruption were encountered, apparently due to the wide HAZ inherent with this technique. While sound welds can be made, some authors[13] reported reduced joint strengths.

Nevertheless, fusion welding of ODS alloys may be useful for making joints in areas that are subject to relatively low stress, since it can be practiced more easily than some of the other processes discussed later, and the joints readily can be inspected.

5. LASER WELDING/ELECTRON-BEAM WELDING

5.1 PROCESS DESCRIPTION

A major advantage of laser welding is the high power density available, which permits small heat-affected zones (spot sizes down to 0.2 mm), precise control of heat input due to the ability to focus the beam, and high rates of heating and cooling. The heat input can be continuous or pulsed; short pulses are used to weld thin materials, whereas a continuous beam is used for deep welds. A high-quality joint is produced. A major attribute is that the laser beam can be transmitted through air rather than requiring a vacuum. The flexibility in processing possible from control of the heat input and precise placing of the beam is readily exploited through automation and robotic machinery.

The ability to focus the beam in electron-beam (EB) welding also allows fusion joints to be made at a significantly lower level of heat input than with typical fusion processes. As with laser welding, the heat-affected zone is small and rapid cooling of the workpiece is possible. A disadvantage is that welding is carried out in a vacuum, which brings limitations of size and shape of the workpiece, and requires additional precautions where degassing of the melt pool will be an issue. Developments in gun technology have made possible EB welding under in a 'soft' vacuum (of the order of 0.1 torr), which significantly reduces the set-up time and allows the use of larger welding chambers. A disadvantage is that the use of a soft vacuum significantly reduces the maximum stand-off distance from the workpiece and decreases the maximum thickness of material that can be joined. 'Out-of-vacuum' EB welding also is possible, which removes any constraint on the size of workpiece but necessitates a further reduction in stand-off distance and maximum thickness of material to be joined.

5.2 APPLICATION TO ODS ALLOYS

Despite the smaller fusion zones possible with the high energy densities possible with laser beams, the features usually associated with fusion joining of ODS alloys of dispersoid agglomeration and microstructural disruption can still occur to reduce the strength of the joints. Nevertheless, the strongest fusion-welded joints reportedly are produced by the application of high energy density lasers (and by electron-beam welding);[12] MA956 retained 40-50% of the stress rupture strength of the parent metal at 1093°C. Laser-welded sheet (0.5 mm thick) of recrystallized PM2000 was reported to retain 57% of the longitudinal tensile strength of the parent metal when tested at 980°C, and 59% in the transverse direction.[14] Improved dispersoid retention in the fusion zone reportedly was observed when MA956 was modified with 1.1-1.9% Ta.[12]

EB welding is distinguished by rapid heating and cooling rates during the melting and solidification processes, which are favorable for minimizing agglomeration and coarsening of the dispersoid during welding of ODS alloys. Also, since the beam energy in EB welding can be regulated over a wide range, this technique can be used to join thick and thin cross sections. The most satisfactory joints in ODS sheet material produced using EB (or laser) welding have involved lap configurations with the beam oriented at a very low angle to the plane of the joint to minimize the fusion-affected zone, hence the extent of effects on the dispersoid and alloy grain structure. Seam-welded lap joints in MA956 reportedly exhibited greater than 40% of the stress rupture strength of the parent metal at 1093°C.[13]

Laser welding has been applied to the fabrication of the honeycomb structures used as abradable tip seals in gas turbines.[15] Alloy foil was corrugated into a half-hexagon shape, after which the strips were laser welded to form a full hexagon shape, and the honeycomb structure was built up layer by layer. Comparative testing of PM2000 (in foil thicknesses of 90, 125, and 150 μm) and Haynes 214 (Ni-16 Cr-14.5 Al-3 Fe-0.01 Y, in wt. % as 130 μm thick foil) in isothermal oxidation in air at 1100-1430°C, and cyclic oxidation involving rapid heating (>500°C/min. to 1220°C) then rapid cooling to room temperature after 1 h exposure suggested that a critical foil thickness in excess of 100 μm would be required for PM2000 for operation at temperatures greater than 1200°C.

Hedrich et al.[14] reported that solidification and crystallization of the weld pool in EB welds made in recrystallized ODS FeCrAl alloys usually proceeds by epitaxial growth of the base material into the fusion zone. The resulting microstructure of an EB joint made in alloy PM2000 is illustrated in Fig. 1, which indicates that the elongated grain structure of the alloy was only slightly changed in the fusion zone. Some small, essentially equiaxed grains formed in the middle of the joint, and partial disarrangement of the typical elongated, high aspect-ratio grain structure in the alloy near the joint by the residual solidification of the weld pool, also are evident in Fig. 1. No obvious formation of gas porosity occurred. These authors also reported that heat strain cracking and grain boundary cracking in coarse-grained ODS-FeCrAl could be avoided by preheating the parts to be welded.

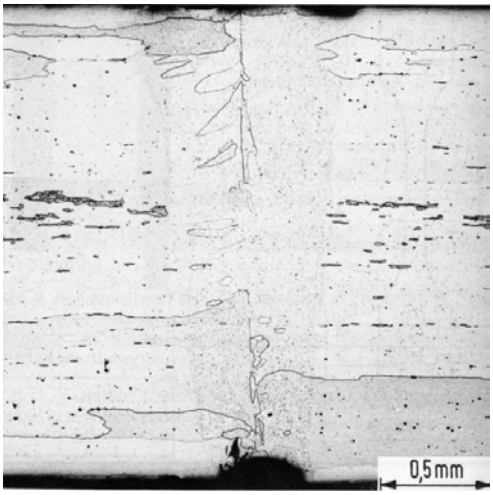

Fig. 1. Micrograph showing typical grain structure in the fusion zone of EB-welded PM2000 sheet, after Hedrich et al.[14]

The typical degradation in tensile properties resulting from EB welding of ODS alloys is illustrated in Fig. 2(a) for coarse-grained alloy PM2000 made from mechanical alloying of completely pre-alloyed master alloy and yttria powder (batch F10L). Although the tensile strength at 1000-1300°C was degraded significantly after EB welding, an additional heat treatment of 1h at 1350°C (the recrystallization temperature of this alloy) improved the tensile strength, apparently through a reduction of the internal stress from the welding process, as well as healing of closed microcracks in the joining zone.

It was found that the strength of joints made by EB welding could be increased by starting with fine-grained PM2000 (prototype alloy F10RK4fP), followed by recrystallization. As indicated in Fig. 2(b), the strength of such joints was 60-70% of that of the monolithic, coarse-grained alloy, significantly higher than for joints made starting with coarse-grained material.[14]

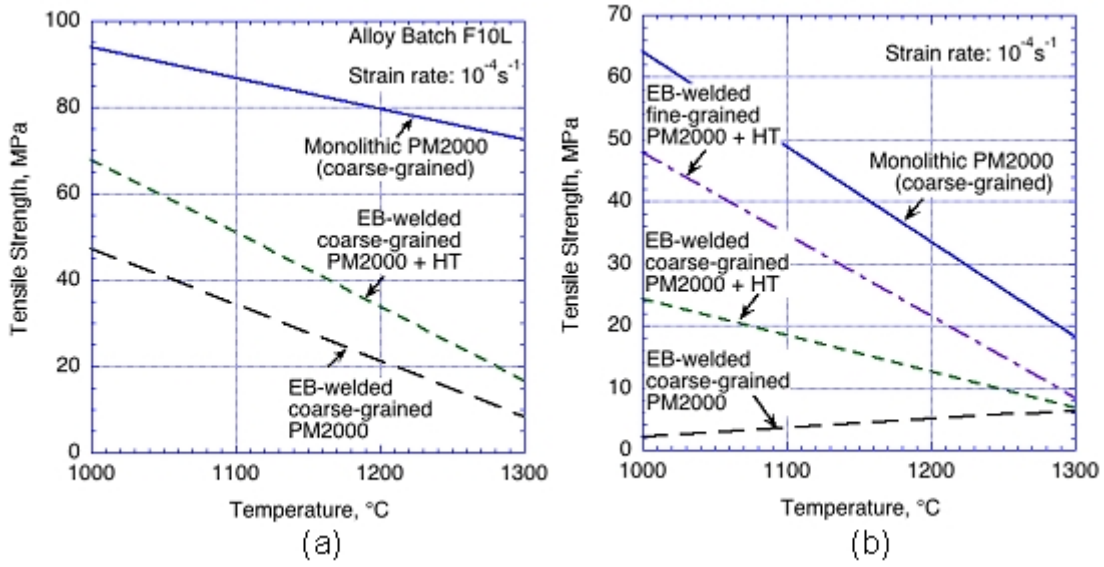

Fig. 2. Tensile strength of EB-welded joints in PM2000 sheet as a function of temperature, compared to the monolithic alloy; (a) alloy batch F10L; and (b) comparison of changes in alloy grain size and post-welding heat treatment, after Hedrich et al.[14]

Holko et al.[7] summarized the strengths (UTS) of fusion welds made in TD-NiCr sheet, as in Table 5. All failures were in the fusion zone of the weld for the UTS values shown.

Table 5. Summary of the ultimate tensile strengths of fusion welded TD-NiCr sheet (after Holko et al.[7])

Process	Thickness mm	Weld configuration	Filler material	Av. Ultimate tensile strength MPa			
				RT	650°C	870°C	1090°C
EB	0.3	Butt	None	710	310	96	34
EB	0.3	Burn-down flange	TD-NiCr	764	—	—	—
GWA	0.3	Butt	None	—	—	—	—
GWA	0.5	Butt, one pass	Hastelloy X	537	—	—	—
			Inconel 62	516	—	—	—
GWA	1.6	Double bevel, 2 passes	Hastelloy X	770	—	—	—

6. BRAZING

6.1 PROCESS DESCRIPTION

Brazing can be used to join metals of the same or dissimilar composition through the use of a filler metal with a melting temperature above 450°C, but below the melting point of the metals being joined. A brazed joint often results in a metallurgical bond that is generally as strong or stronger than the base metals being joined. In furnace brazing, temperatures of 1120 to 1150°C and typically used to braze stainless steels with Ni-based filler metals, or carbon steel with Cu filler metal.[16,17]

In furnace brazing, the parts or assemblies being joined are heated to the melting point of the filler metal being used, allowing the molten filler metal to flow via capillary action into the close-fitting surfaces of the joint and form an alloy of the materials at the transition point upon solidification. The base metals do not melt, but they can alloy with the molten filler metal by diffusion to form a metallurgical bond.

Because the metallurgical properties at the brazed joint may differ from those of the base metals, the selection of the appropriate filler metal is critical. Some filler metals are characterized by melting point depressant additions. After brazing, the MPt depressant tends to diffuse away from the joint, restoring the melting temperature of the joint to that of the base alloy. Typical additions used are Si, B and P; the selection of the appropriate MPt depressant depends on multiple factors—for instance, Si could react with Cr and Mo to form intermetallic hard and brittle phases.

Certain Ni-base precipitation-hardenable superalloys contain substantial proportions of Al and Ti that provide the precipitation phases. Since the oxides of these elements are almost impossible to reduce in controlled atmospheres available during brazing (vacuum or hydrogen), the surfaces to be brazed must be precoated with a thin layer of electroplated Ni to allow wetting by the filler metal.

6.2 APPLICATION TO ODS ALLOYS

The overall state of knowledge of brazing and soldering of ODS alloys has been summarized by O'Donnell.[18] As Special Metals Corp.[6] emphasized that successful brazing, diffusion bonding and transient liquid phase (TLP) bonding of ODS alloys which contain high levels of Cr and Al requires extreme care to remove the protective alumina film. In addition to forming unwanted oxide films, oxidation during brazing may inhibit the flow of the filler metals. Approaches include grinding followed by chemical cleaning, or pre-plating with a thin layer of Ni to minimize oxidation during joining. The bases used for filler metals for ODS alloys must be capable of withstanding temperatures in the range of 1230 to 1315°C after the melting-point depressant elements have been diffused away, to allow typical processing operations such as secondary recrystallization, and high service temperatures, so that candidate filler alloys typically are based on Ni, Co, Au or Pd. However, some authors expressed concern that the maximum operating temperature for such brazed joints will be sufficiently lower than the required operating temperatures (for MA754, for instance; Kelly)[19] that for joints for ODS alloys really should be made by methods other than brazing.

Ni-based alloys with high levels of low-melting additions such as Si and B often are preferred for brazing ODS alloys in order to avoid excessive melting of the base metal and the corresponding agglomeration of the oxide dispersion. Examples of brazing filler metals are given in Table 6.[7,13] Note that TD-6 has essentially the same composition as alloy

Hasteloy C, with the addition of 4% Si to depress the melting point and provide good wetting and flow characteristics to enable brazing at 1300°C. This alloy has been used extensively in the brazing of TD-NiCr honeycomb structures and other gas turbine components.

Table 6. Examples of brazing filler alloys used with ODS alloys (after Holko et al.[7])

Alloy	Est. brazing T, °C	Nominal composition (wt%)										
		Ni	Cr	Pd	Al	Si	B	Au	Mo	W	Fe	Co
TD-5	1065	Bal	22	—	—	4	—	—	9	—	22	1.5
TD-6	1315	Bal	16	—	1	4	—	—	17	5	4-7	—
TD-20	1300	Bal	16	—	—	4	—	—	25	5	—	—
Ni-Pd	1300	Bal	—	60	—	—	—	—	—	—	—	—
J8100	1245	Bal	19	—	—	10	—	—	—	—	—	—
Palniro 1	1175	25	—	25	—	—	—	50	—	—	—	—
AMS 4779 (CM50)	1175	Bal	—	—	—	4	2	—	—	—	—	—
Palniro 7	1065	22	—	9	—	—	—	70	—	—	—	—
TD-50	1065	Bal	20	—	—	10	—	—	9	—	21	2 max
NX77	1175	Bal	5	—	—	7	1	—	—	1	—	1
N58	1190	Bal	—	—	—	2	1	—	—	—	—	—
B93[a]	1290	Bal	14	—	3	5	1	—	4	4	—	9

[a]Also 4.9 Ti.

However, such high brazing temperatures can lead to significant 'erosion' of the component being brazed, which is a major concern for thin-walled structures. There is also the possibility for metallurgical interaction between the work piece and the braze, leading to interdiffusion, porosity, and disruption of the dispersoid. The use of large overlaps in joints brazed using TD-6 typically result in failure in mechanical testing occurring in the parent metal. As a result, the results of creep-rupture testing of such joints often are difficult to interpret. Figure 3 shows some such data for 1.6 mm-thick TD-NiCr sheet brazed using TD-6. At 1090°C, the joints failed in the parent metal, whereas at 1204°C the failures were in the braze.

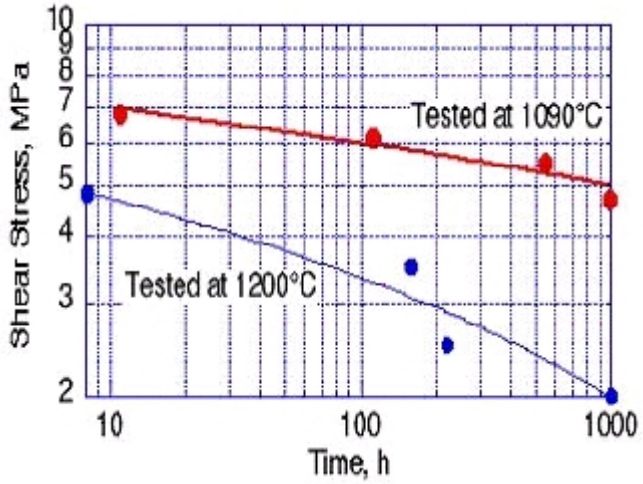

Fig. 3. Comparison of creep-rupture shear strengths at 1090 and 1204°C of brazed lap joints in TD-NiCr sheet made using braze alloy TD-6 and an overlap of 1.6 mm (as summarized by Holko et al.[7]).

Brazing was one of several, approaches used for the assembly of a radiant air heater made from the Ni-based ODS alloy Inconel MA754.[20, 21] The assembly of the heat exchanger is shown schematically in Fig. 4, and consisted of MA754 tubes, together with elbows and end plates that were machined from MA754 blocks. The tubes also contained internal swirlers machined from Inconel 625, to promote heat transfer within the tubes. The approaches that were examined for joining the mechanically alloyed components were:

- threading,
- bonding,
- metallurgically-sealed threads, and
- mechanically-sealed threads.

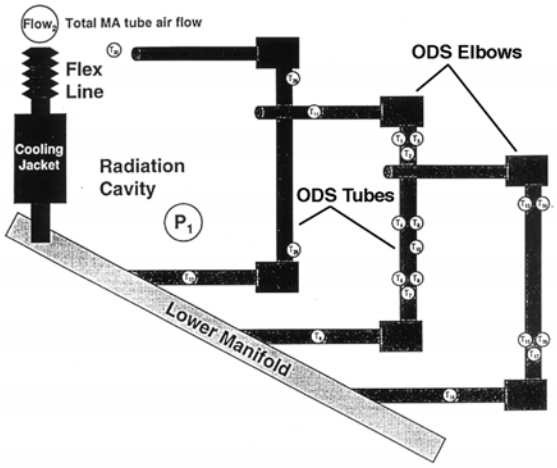

Fig. 4. Schematic cross section of an ODS heat exchanger (after Seery and Sangiovanni et al.[20]).

Threads were machined in a number of trial components, with male threads on 25 mm diameter rods, and corresponding female threads machined into the blocks that represented the elbows.

Although MA754 exhibits a tendency to gall, Class 1 threads resisted galling. The use of high-temperature gaskets for sealing was investigated, but rejected since the coefficient of thermal expansion of the commercially-available materials was less than that of the MA754, such that there was a gap present at elevated temperatures. Metallurgical sealing of threaded members was evaluated, as well as conventional sleeve brazing.

Based on the results of these tests, the joint configuration shown schematically in Fig. 5 was chosen, with brazing as the method of joining. The composition of the brazing alloy used was Ni-9.5Cr-3.0Al-4.9Ti-7(Mo+W) + 4.5Si + 0.7B, and its melting point was 1038°C. The initial brazing operations were performed in a large vacuum furnace at 1052°C. The configuration was held at temperature for approximately 45 minutes, then heated to 1232°C and held at temperature for an additional 255 minutes prior to furnace cooling. In order to facilitate the brazing process, a jig was constructed that allowed the tubes, elbows, and end plates to be assembled and held in position with a minimum of movement. The resulting high-temperature air heater successfully demonstrated the ability to heat air from 704-982°C.[14]

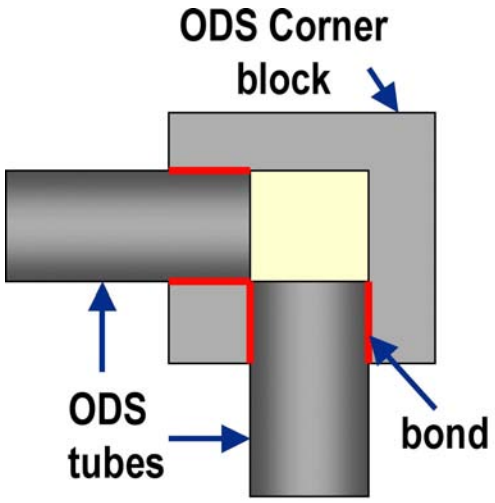

Fig. 5. Schematic representation of the joint configuration used in Ref. 20.

Effort in a European program (COST 522) explored brazing of PM2000 to itself, and to a Ni-based alloy 45-TM (Ni-27Cr-23Fe-2.7Si-0.1Rb) to simulate a dissimilar metal joint.[22] Three commercial filler metals were used: BNi-5 (Ni-based); Pd-40Ni; and Ag-4Ti. This selection was based on anticipated strength and oxidation resistance at the desired testing temperature of 800°C. The composition and melting temperatures of these brazing alloys are shown in Table 7. Although the starting point for the manufacture of specimens was vacuum brazing, volatile elements (such as Ag and Cr) in the base or filler metals necessitated the use of an elevated chamber pressure to prevent excessive loss during operation. For some base material/filler metal combinations, it was necessary to mask specimen surfaces outside the joint area with a ceramic stop-off material to prevent excess filler material flowing along the specimen surface.

Table 7. Nominal compositions and brazing parameter ranges used in COST 522[22]

Alloy	Composition (wt %)	Melting T (°C)	Brazing T (°C)	Brazing time (min)	Atmosphere
PM2000	See Table I	1480	1000-1250	0-120	vacuum, Ar
45-TM	See Table I	1390	1000-1250	1-120	vacuum, Ar
Ag-4Ti	Ag-4Ti	950-960	1000	3	vacuum, Ar
BNi-5	Ni-19Cr-10Si	1079-1135	1080-1220	1-120	vacuum, Ar
Pd-40Ni	Pd-40Ni	1237	1250	39507	vacuum

The brazed joints were evaluated in short-term shear testing at a constant displacement rate (for optimizing the brazing parameters and specimen design) in air at up to 900°C; shear creep testing of the joints under constant load in air up to 800°C; and multi-axial creep tests of the tubular specimens under constant internal argon pressure up to 800°C. The configuration of the specimens used is shown schematically in Fig. 6. The specimen design for shear testing aimed to retain simple shear as far as possible. However, some dimensional modifications were required during the program, since lap joints that were too long resulted in base material failures in short- term testing, and lap joints that were too short produced creep shear failure surfaces that were difficult to quantify for the original joint area because of oxidation. The specimen for the internal pressure creep testing used similar cross-sectional dimensions (38 mm diam. x 4 mm thickness) as the components of industrial heat exchangers. A single brazed butt joint was included in the mid-section, and threaded end plugs (type 316 stainless steel) sealed by brazing. A gas inlet tube was connected to one of the end plugs.

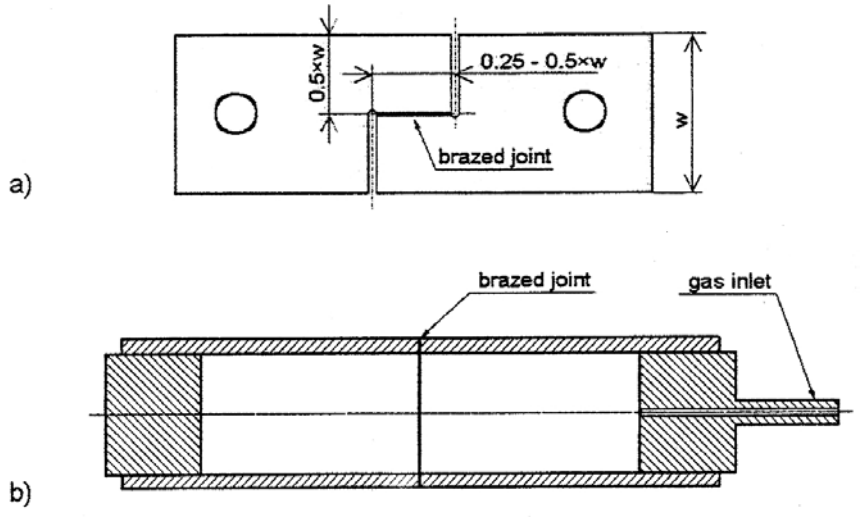

Fig. 6. Specimens used for (a) shear creep testing, and (b) for internal pressure creep testing (after Holstrom et al.[22]).

Graphite fixtures were used for the shear testing specimens, and some masking of the fixtures also was required. The internally-pressured creep specimens were self-aligning and self fixturing. Ultrasonic inspection using C-mode scanning acoustic microscopy (C-SAM) was used to investigate the joint integrity in the specimens before and after testing.

The test results of the short-term shear strength tests indicated that the service temperature of the joints with the Ag-4 Ti filler material would be limited to below 600°C. As a result, this filler material was discarded. The joints brazed with BNi-5 and Pd-40Ni filler materials showed good short-term strength up to 900°C, and similar temperature-dependence of strength when compared with the base material. At the highest testing temperatures (900°C), the joints in the 45-TM reference material showed similar strength values as joints in the ODS alloy.

In the shear creep strength testing, the actual shear stresses experienced were estimated from the fracture surface areas. Figure 7 shows the results for the filler metal BNi-5. In all tests with this filler metal, the specimen failed at the joint, with the fracture front advancing through both the filler metal and the interfacial zone between the filler metal and the base alloy. In all cases, the 45-TM reference alloy showed considerable plastic deformation at fracture, whereas the ODS alloy all base metal combinations (PM2000 to PM2000, 45-TM to 45-TM, PM2000 to 45-TM) were included) showed practically none. The shear creep strength of Pd-40Ni filler metal brazed joints was somewhat higher than for the BNi-5 at 800°C, but the difference between these two brazes was insignificant at a shear stress of less than 25 MPa.

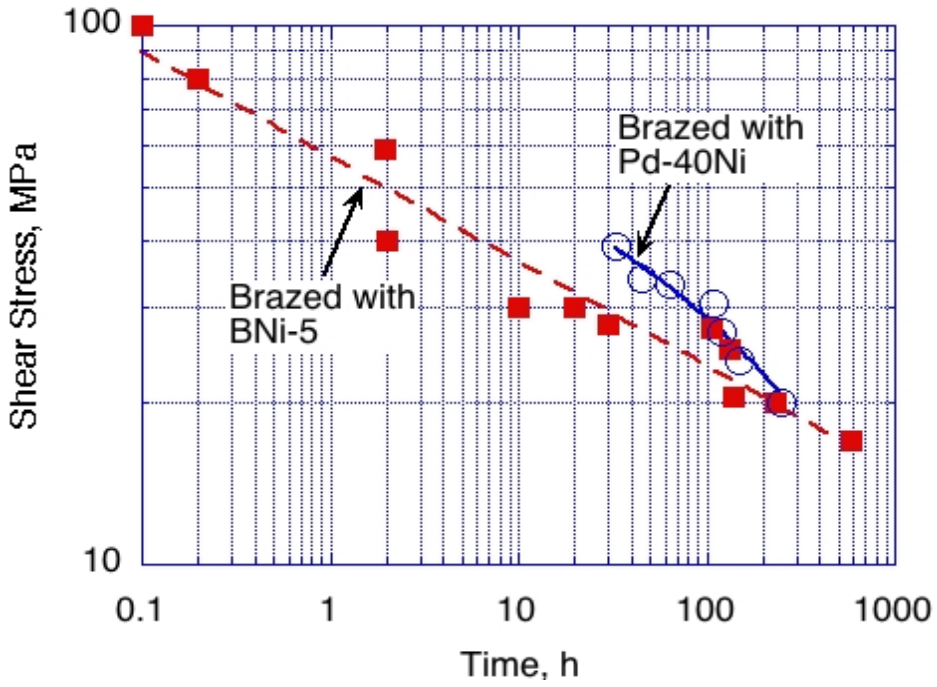

Fig. 7. Shear creep strength for BNi-5 and Pd-40Ni brazed joints at 800°C (after Holstrom et al.[22]).

The results for the internal pressure creep strength tests, performed with tubular PM2000 specimens and Pd-40Ni brazed joints, are compared in Fig. 8 with the shear creep test results from all base material combinations brazed with the same braze. Ultrasonic inspection using C-SAM showed that a sound butt joint could be achieved using a Pd-40Ni braze. In those cases where the joining had not been totally successful, the C-SAM correctly detected the location of small leaks. In the specimens that failed in the joint, the failure was due to a too-tight insert during brazing, which resulted in a very thick joint. In the specimen that failed prematurely in the base material, similar inhomogeneity was suspected. Despite initial difficulties in producing perfect gas tightness for the test joint and the end plugs, these results suggested that sufficient creep strength can be achieved with this joining approach to allow satisfactory application in practical components. In a European BRITE/EURAM Project (No. BE97-4949), intended to develop heat exchanger tubes capable of operation at 1100°C or higher, involved the design of a novel high-temperature heat exchanger in which the radiant section used panels of free-hanging PM2000 tubes (~6m long) for the walls of the furnace section.[23] A bayonet-type tube arrangement was chosen so as to take advantage of the temperature capabilities of the ODS alloy, while accommodating its mechanical limitations. This design enables straight sections of PM2000 to be used, and minimizes the amount of material required. The tubes are top-supported, and are allowed to expand individually without constraint. To facilitate assembly and tube exchange, the tubes are connected to the header by a threaded connection piece. In the resulting design, there is no physical connection between the individual PM2000 tubes and the tubes that transport the heated air to the header outlet. The air to be heated flows between the annulus created by the ODS tube and the inner gas return tube (which is made of a ceramic material), and then passes through the inner ceramic tube to the exit manifold.

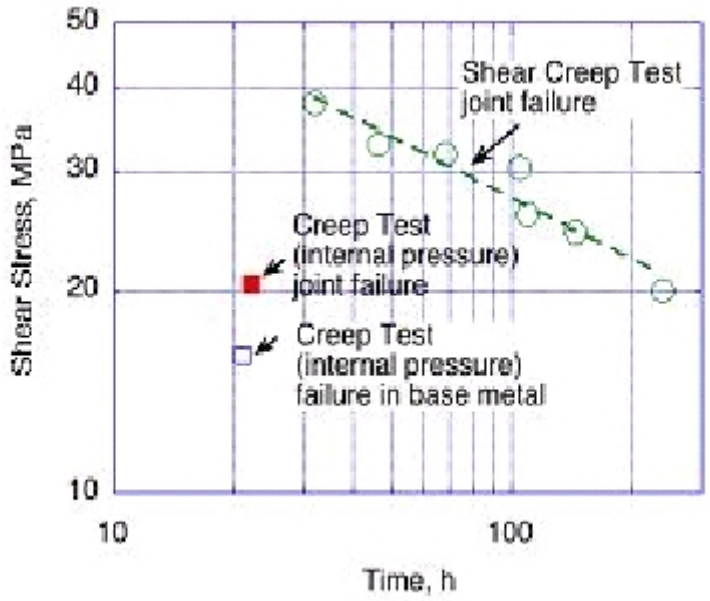

Fig. 8. Internal Pressure Test Results at 800°C with Pd-40Ni-brazed PM2000 tubes (after Holstrom, et al.[22]). (Including shear creep test results from all base material combinations brazed with the same braze.)

Figure 9 illustrates one such heat exchanger design considered in a European BRITE/EURAM Project (No. BE97-4949), intended to develop heat exchanger tubes capable of operation at 1100°C or higher, involved the design of a novel high-temperature heat exchanger in which the radiant section used panels of free-hanging PM2000 tubes (~6m long) for the walls of the furnace section. A bayonet-type tube arrangement was chosen so as to take advantage of the temperature capabilities of the ODS alloy, while accommodating its mechanical limitations. This design enables straight sections of PM2000 to be used, and minimizes the amount of material required. The tubes are top-supported, and are allowed to expand individually without constraint. To facilitate assembly and tube exchange, the tubes are connected to the header by a threaded connection piece. In the resulting design, there is no physical connection between the individual PM2000 tubes and the tubes that transport the heated air to the header outlet. The air to be heated flows between the annulus created by the ODS tube and the inner gas return tube (which is made of a ceramic material), and then passes through the inner ceramic tube to the exit manifold.

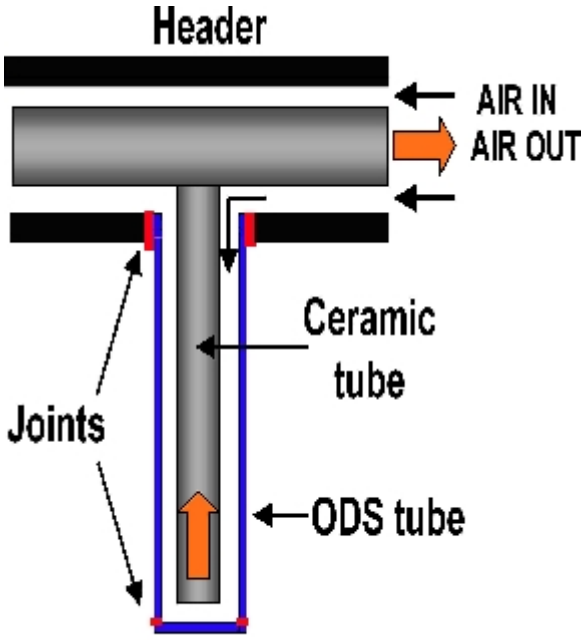

Fig. 9. Schematic representation of a heat exchanger configuration considered in a European Brite-Euram Project (after Olsson et al.[23])

Tabernig et al.[24] used a Pd-40Ni brazing alloy to assemble a spacecraft thermal protection system that consisted of an internal honeycomb structure made of 125 μm-thick foil of PM2000 (strength and lower density), with an outer skin and end plates of 250 μm sheet of PM1000 (higher emissivity due to the formation of a chromium oxide scale). The honeycomb was made by laser welding strips of PM2000 foil that had been corrugated into a half hexagon shape to form the full hexagon shape; the final honeycomb consisted of multiple layers of such strips.[15] The face-sheets and end plates were attached to the honeycomb by brazing in a high-vacuum furnace (<10^{-5} mbar) at 1250-1260°C (MPt. of Pd-40Ni is 1238°C); a typical brazing cycle occupied approximately 5h, with a hold time of

5 to 10 min at brazing temperature. Full-size panels (420 x 300 mm) were assembled by first assembling the component parts on to fixturing by laser spot welding before brazing. The corrugated PM2000 honeycomb was ground to a flatness of <50 µm to avoid missing joints after brazing, and the edges of the honeycomb were cut at a 45° angle. A 50 µm-thick foil of the braze alloy was employed. Test samples cut from the completed panels were subjected to a series of engineering tests. No damage, or change in surface flatness was observed after a series of thermal cycling tests in which the face sheet was heated to 1050°C at progressively increasing heating rates (5°C/s to 40°C/s). The structure also successfully passed 50 cycles of testing involving combined mechanical and thermal loading simulating the conditions expected during ascent and re-entry of a space vehicle. In a final test at 1100°C, the mechanical load was increased until failure occurred. The structure failed at the point of maximum bending moment at a load that was approximately 10% higher than the predicted failure point (1167 N), and apparently was initiated by dimpling of the compressed face sheet.

Solar Turbines, Inc. reported that gas turbine fuel injector tips made from PM2000 (and MA754) were successfully brazed to a Hastelloy X center body,[25] though the braze(s) used were not specified. Brazed PM2000 was selected for further evaluation, and reportedly the performance was sufficient for the process to be considered for application in several other models of gas turbine.

7. RESISTANCE WELDING

7.1 PROCESS DESCRIPTION

Resistance butt welding is the simplest version of a group of resistance-welding processes that involve the application of heat and pressure in the area to be joined. The heat is generated from the resistance to the passage of a high electric current through metal parts held together under a pre-set pressure. The faces of the pieces to be joined may be flat and parallel or, in the case of larger sections, profiled to reduce the initial contact area and further concentrate the heating at the interface. Typically, the components are clamped in opposing copper dies, with a short length of each component protruding, and abutted under pressure. Current is passed between the dies, causing resistance heating of the contact area, the heat generated depending on the current, the duration of the current, and the electrical resistance of the component pieces. Since the resistance is highest at the joint interface to be joined, heating is most intense in this area. As the component ends heat up and soften, deformation occurs to an extent that depends on the applied load, resulting in forging without the necessity of melting. The current is terminated after a pre-set duration, or once a pre-set length has been upset. The joint typically is cooled under pressure, before being released from the fixturing. The deformation in the weld-upset zone may be left in place or removed, depending on the requirements.

7.2 APPLICATION TO ODS ALLOYS

Resistance welding of ODS alloys has been used predominantly to make butt joints in wires and rods up to approximately 16mm diam.[26,27,28] The principle of hot forging associated with resistance welding originally was used to join 13%Cr ferritic ODS steels DT2906 and DT2203Y05 (see Table 1), but later was adapted for joining ODS end plugs to tubes for use as reactor fuel pins in the French fast breeder reactor project.[10] The process employed a special resistance-welding machine designed at the Belgian Nuclear Research Centre in Mol (SCK/CEN). The welding was performed inside a glove box, but it is not clear if this was a requirement of the joining process, or because the tube to be capped contained fuel and blanket pellets. No post-joining testing was reported. However, a micrograph of the tube-to-plug joint showed a relatively small amount of disruption of the microstructure of the tube (Fig. 10). Further developments of this technique were described by Bottcher et al.[29]

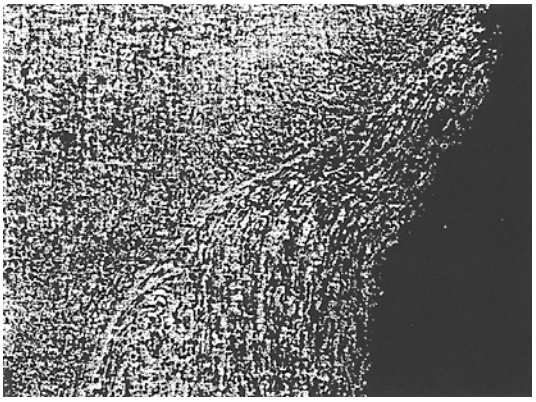

Fig. 10. Cross Section of Cap-to-Tube Joint in MA957.[10]

7.3 FLASH BUTT/RESISTANCE FORGE WELDING

This technique combines high temperatures obtained by resistive heating of the parts to be joined with intense plastic deformation of the bond interface to disrupt surface contamination and provide a driving force for recrystallization across the interface. The deformation occurs over a period of up to tens of seconds. In flash butt welding, the flashing action is created by high current densities at small contact points between the faying surfaces, and expels material from the joint as the surfaces are forced together. The final rapid upsetting of the surfaces creates a metallic bond. For alloy MA956 proper adjustment of the upset parameters was key to achieving defect-free bonds;[30] the best results were obtained when the upset force was maintained for approximately 10 sec. after the target upset distance was achieved. Forging continued for several seconds after the upset current was turned off. Processing conditions involving shorter flashing times and greatly-reduced upset currents, compared to other Fe- and Ni-based alloys, produced clean bond lines, as illustrated in Fig. 11. The distortion of the alloy microstructure, and the difference in alloy grain size in the heat-affected zone (HAZ) and the unaffected alloy are clearly evident in Fig. 11(b), and are similar to those produced in inertia friction welding [see Section 10.3]. Brown et al.[30] also reported that good welds were produced in all combinations of joints between fine-grained and recrystallized MA956, and with Inconel 601.

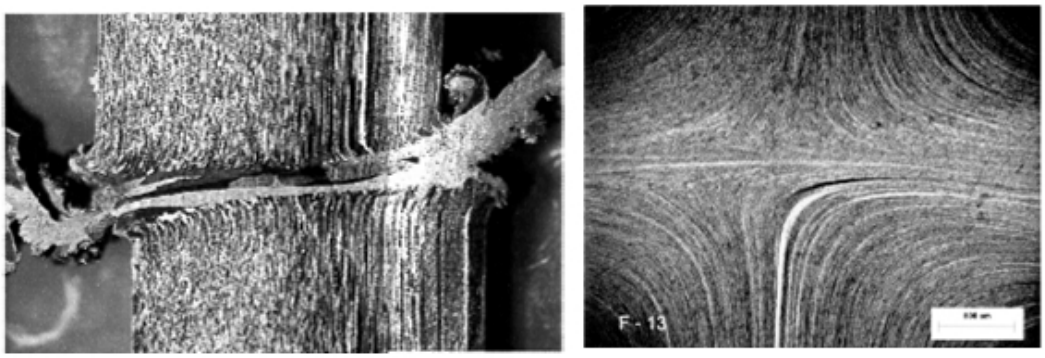

Fig. 11. Cross section of MA956 joined to itself using flash butt welding (a) macro image of a typical weld; (b) microstructure of a weld made using increased flashing acceleration and reduced upset current.[30]

The results of tensile tests of joints in fine-grained MA956 are shown in Table 8; the as-welded joints were relatively weak, retaining a maximum of 36% of the UTS, and 24% of the YS. Post-welding recrystallization resulted in a notable increase in tensile strength, to 42% of UTS, and 49% of YS. Failure typically occurred in the HAZ regions following necking, not in the bond lines. The location of failure appeared to coincide with the maximum change in grain orientation and growth.

Table 8. Results of tensile tests at 982°C (strain rate of 0.127 mm/min) for fine-grained MA956 joined to itself by flash butt welding[30]

Specimen No.	UTS (MPa)	0.2% YS (MPa)	Elong. (%)	RA (%)
Fine-grained condition (not recrystallized)				
Parent-1	108.2	94.5	8.5	15
Parent-2	108.9	92.4	8.5	24
Parent-3	106.2	88.9	8.0	23
FBW 12-1	38.6	19.3	—	38
FBW 12-2	28.3	22.1	—	29
FBW 12-3	29.0	21.4	5.0	25
FBW 13-1	28.3	19.3	—	28
FBW 13-2	29.0	19.3	—	27
FBW 13-3	29	21.4	—	29
FBW-1	38.6	19.3	—	38
FBW-2	28.3	22.1	—	29
FBW-3	29.0	21.4	5	25
FBW-4	28.3	19.3	—	28
FBW-5	29.0	19.3	—	27
FBW-6	29.0	21.4	—	29
Recrystallized at 1375°C for 1 h				
FBW-1	44.1	44.1	1	7
FBW-2	45.5	45.5	1.5	7.5

The application for which the forge welding process was developed was cap-to-tube joints for breeder reactor fuel pins, and the components used in the evolution of the joining parameters consisted of a simulated end cap, a restraining ring, and a simulated cladding tube, as indicated in Fig. 12.[31] As indicated, the simulated end cap had a land with an outer diameter (2 mm) slightly larger than the internal diameter of simulated tubing, and a tapered section to expand the tube on insertion. The restraining ring provided the backing force for plastic deformation of the interface, and had an internal diameter machined to match the computed outside diameter of the tubing after expansion by the inserted end cap. Experience resulted in the addition of 0.2 mm shim stock between ring and tube. The joining procedure was conducted using a Gleeble machine, and involved inserting the simulated end cap into the simulated cladding to a depth of 9 mm cold, then heating to

1000°C before inserting to the full distance of 16 mm, then cooling while under compressive (axial) load.

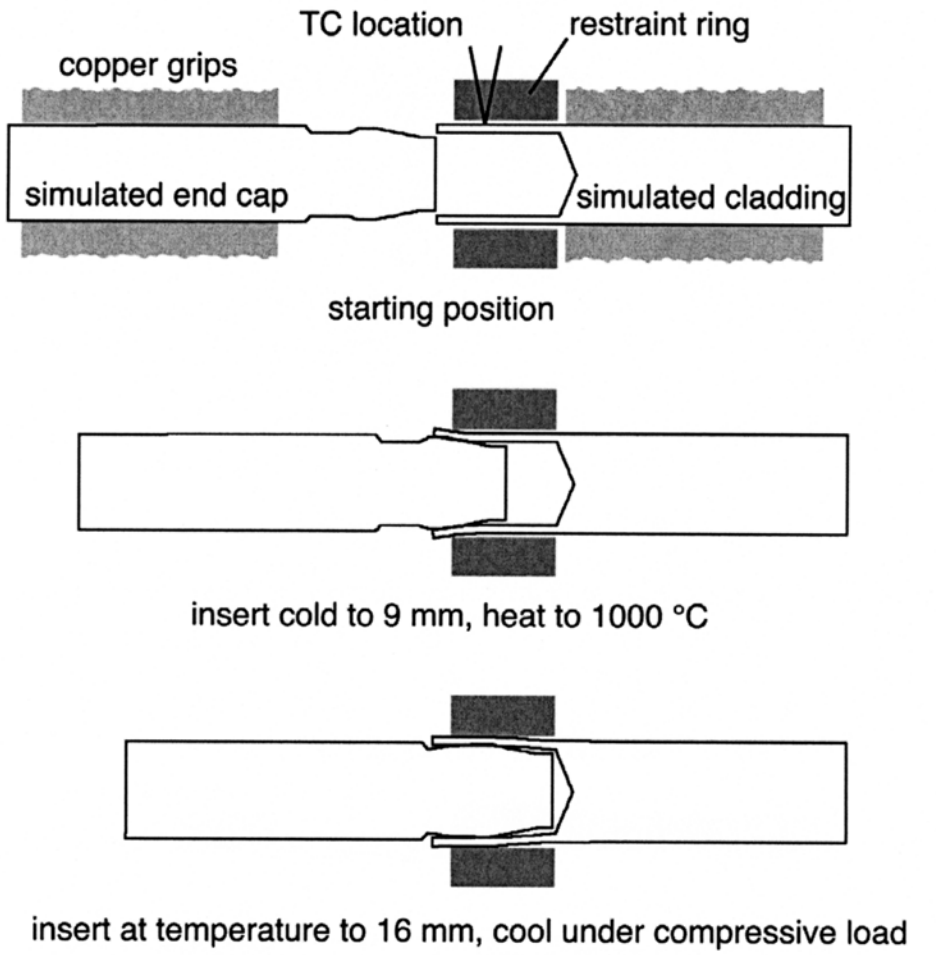

Fig. 12. Schematic representation of joining procedure used in resistance forge welding trials.[31]

Figure 13(a) shows a macro-section of such a bond made using fine-grained PM2000, and Fig. 13(b) shows an unetched cross section of the upper weld, which indicated full bonding. The short cycle time and (relatively) low temperature involved were insufficient to cause secondary recrystallization of the alloy, and the existing fine grain size was not resolved by etching. Tensile tests (performed in the Gleeble machine) gave the results listed in Table 9. The optimized welds made using this configuration were repeatable, and in tensile testing failures occurred in the tubing away from the weld.

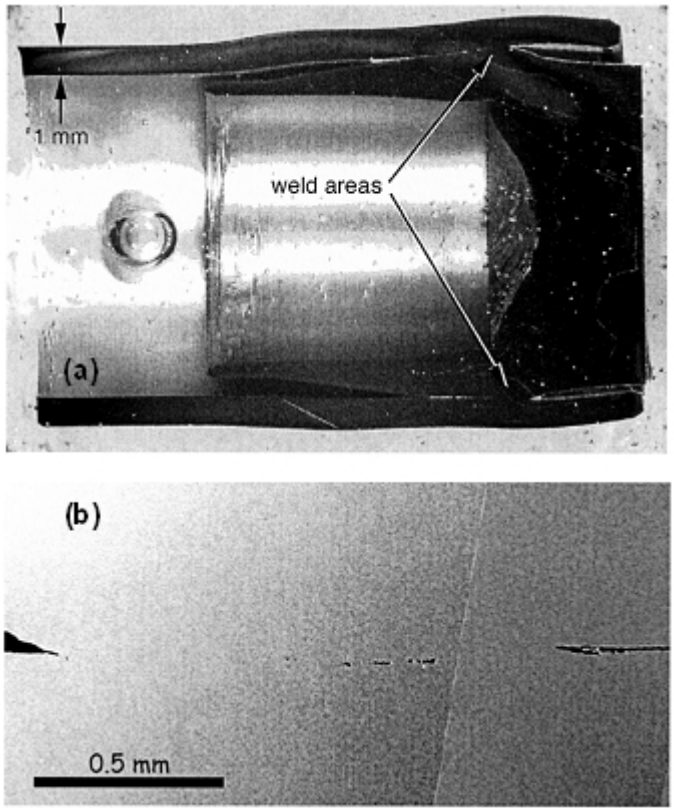

Fig. 13. Cross section of a typical resistance forge weld showing (a) macro-view of joined simulated end cap and tube (sectioned and polished surfaces appear dark); and (b) view of the unetched welded surface.[31]

Table 9. Tensile test results for welds in fine-grained PM2000 by resistance forge welding[26]

Insertion distance, mm	Test temperature, °C	Axial load, kg	Cladding wall stress, MPa	Corresponding internal pressure, bar
15	20	1036	270.3	1103
	900	541	144.1	589
16	20	3610	961.1	3930
	900	542	144.1	590

7.4 TORSIONAL RESISTANCE FORGE WELDING

This processing variant utilized the capability for controlled axial and torsional motion afforded by a torsional Gleeble unit to provide increased levels of deformation at the interfaces to be joined[31] (see, also, Section 10.3 on Inertia-Driven Friction Welding). Despite difficulties in developing fixturing to provide accurate alignment of the components, procedures were developed that produced reasonably well-aligned joints in fine-grained PM2000 (see Fig. 14). The conditions used were an axial load of 100N at 850°C, and torsional motion of +30°, -60°, +60°, -60°, and +30° over 4 s. The key changes were to reduce the axial loading and to apply torsional loading intermittently (several rotations of 60° compared to making a full turn in one direction). Metallographic examination indicated that complete bonding was achieved, but no detailed micrographs were presented and no mechanical testing was reported, apparently because the process was not sufficiently developed. Nevertheless, this process was considered to have the potential for producing acceptable end cap-tube joints relatively inexpensively.

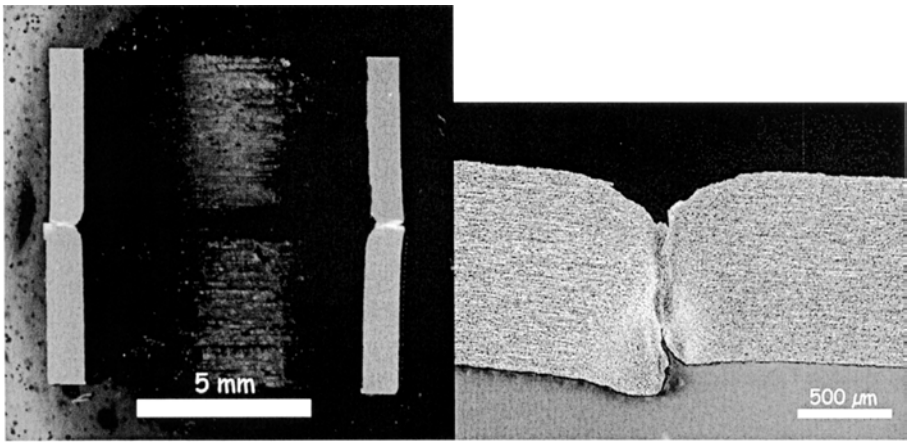

(a) **(b)**

Fig. 14. Cross section of a torsional forge weld showing (a) macro-view of joined tube); and (b) view of a welded surface (etched[31]).

7.5 RESISTANCE SPOT WELDING

Extensive efforts to use resistance spot welding for TD-NiCr sheet intended for space shuttle skin applications have been summarized by Holko et al.[7] Sound, defect-free spot welds have been made in foil/sheet thicknesses ranging from 0.08 to 1.5 mm. Both fusion and solid-state spot welding were successful. The welding parameters, and the resulting tensile shear strengths are summarized in Table 10, while the 100-h creep rupture strengths at 1090 and 1204°C are indicated in Table 11.

The microstructure of a typical fusion spot weld in TD-NiCr shown in Fig. 15 was considered to be representative of those that result from the use of the spot welding parameters listed in Table 10. While the quality of the available micrographs is less than desired, there appear to be areas of recrystallized grains in the vicinity of the weld line (Fig. 15c).

Table 10. Summary of resistance spot-welding process parameters and resulting tensile shear strengths (after Holko et al.[7])

Sheet Thickness (mm)	Spot Diam (mm)	Weld Type	Surface Prep.	Machine Type	Electrodes		Pneumatic Force (kN)	Current (kA)	Machine Settings				Tensile-Shear Properties (MPa)					
					Class	Contact face (mm radius)			% Heat	Weld cycles	Cool cycles	No. pulses	RT		1093°C		1204°C	
													Load (kN)	Shear stress	Load (kN)	Shear stress	Load (kN)	Shear stress
0.8	5.8	solid state	—	3-phase	III	203	13.4	—	37	10	1.5	12	8.46	310	—	—	1.05	41.4
0.25	2.7	fusion	solvent wipe		III	100	4.45	35	65	2	—	1	1.31	210	—	—	—	—
0.63	6.3	solid state	200 grit, degrease, acetone wipe		II	6.4	8.9	18.9	27	3.5	2.5	40	6.09	190	0.83	31.8	0.7	25.7
1	6.8					8	13.4	25.9	37	3.5	2.5	42	9.3	292	1.08	29.7	0.97	24.8
0.63	4.8			1-phase	III	203	2.45/6.67	14.3	65	2	1	60	3.51	192	0.25	13.8	—	—
1	4.8						2.22/7.11	16.3	70				4.59	259	0.42	22.8	—	—
0.63	4.8	fusion					2.67/7.11	15.7	70				4.96	247	0.65	33.1	—	—
1	5.8							17.4	75				8.65	323	1.05	40	—	—
1.5	6.6							22.1	95				12.1	343	1.23	35.2	—	—
0.51	4.1		solvent wipe	3-phase	—	—	8.9	—	27	7	0.5	1	4.09	318	0.45	34.5	0.33	25.5
	4.3	solid state	#1 Emory paper, acetone wipe	1-phase	—	—	6.68	—	40	7	0.5	50	—	—	—	—	—	—
0.38	4.4	fusion	pickled, store in Freon		III	203	10	28	28	1	—	1	3.15	208	0.65	42.8	—	—
	5.5	solid state				305		24.2	<20	15	—	1	3.32	141	0.57	23.5	—	—
	5.4[a]							20.1	<20	8	—	1	—	—	—	—	—	—

[a]Specially-processed, unrecrystallized sheet, with post-weld heat treatment.

Table 11. 100-h creep rupture shear strengths for single-spot lap joints in resistance spot-welded TD-NiCr sheet (Holko et al.[7])

Thickness (mm)	Weld type	100-h creep rupture strength			
		1090°C		1204°C	
		Load (N)	Stress (MPa)	Load (N)	Stress (MPa)
0.63	Solid state	702	23	565	18
1	Solid state	610	16	388	10
0.5	Fusion	400	31	—	—
0.5	Solid state	258	17	—	—
0.38	Fusion	423	27	—	—
0.38	Solid state	506	23	—	—

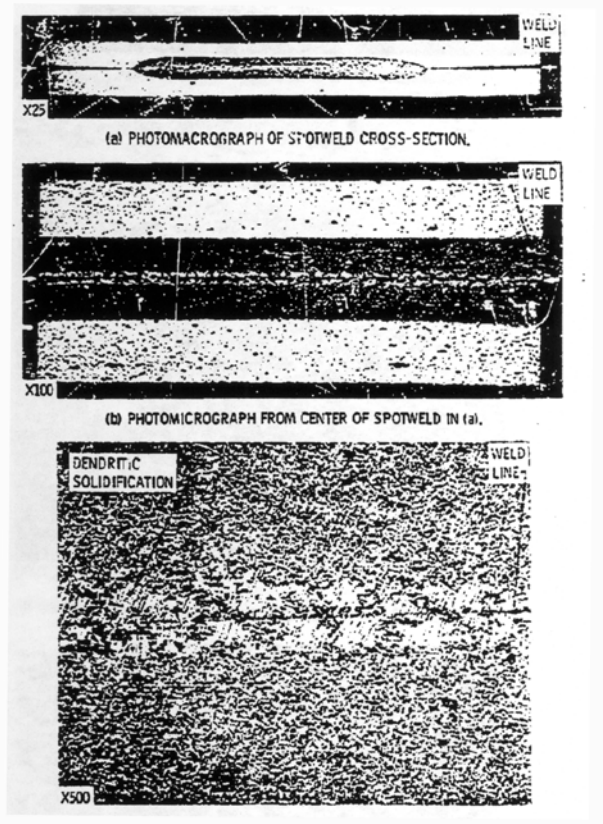

Fig. 15. Cross section of a typical fusion resistance spot weld in TD-NiCr sheet: (a) macro view of the spot-welded cross section (electrolytically etched in 10% oxalic acid); (b) micrograph from the center of the spot weld shown in (a); and (c) higher magnification view from the center of (b) (after Holko et al.[7]).

Reduced melting from the use of a shorter welding time (one cycle of single-phase power) produced microstructures (such as those shown in Fig. 16), in which there was no obvious evidence of localized grain growth. While less melting during welding is considered desirable, the thoria particle distributions in these two microstructures were not measured to provide confirmation. Solid-state spot welding typically resulted in the formation of small, recrystallized grains along the weld line. Apparently, these grains could be eliminated by chemical polishing to remove the asperities and cold-worked layer resulting from surface sanding. Some improvement in bond strength was reported following subsequent heat treating of the welded component. 'Specially-processed' unrecrystallized TD-NiCr sheet, spot welded using the parameters indicated in Table 10, exhibited a microstructure in which the weld line was undetectable after a recrystallization heat treatment of 2 h at 1200°C in H_2 (Fig. 17). This was considered to be the optimum solid-state spot weld;[7] unfortunately, no strength data were reported.

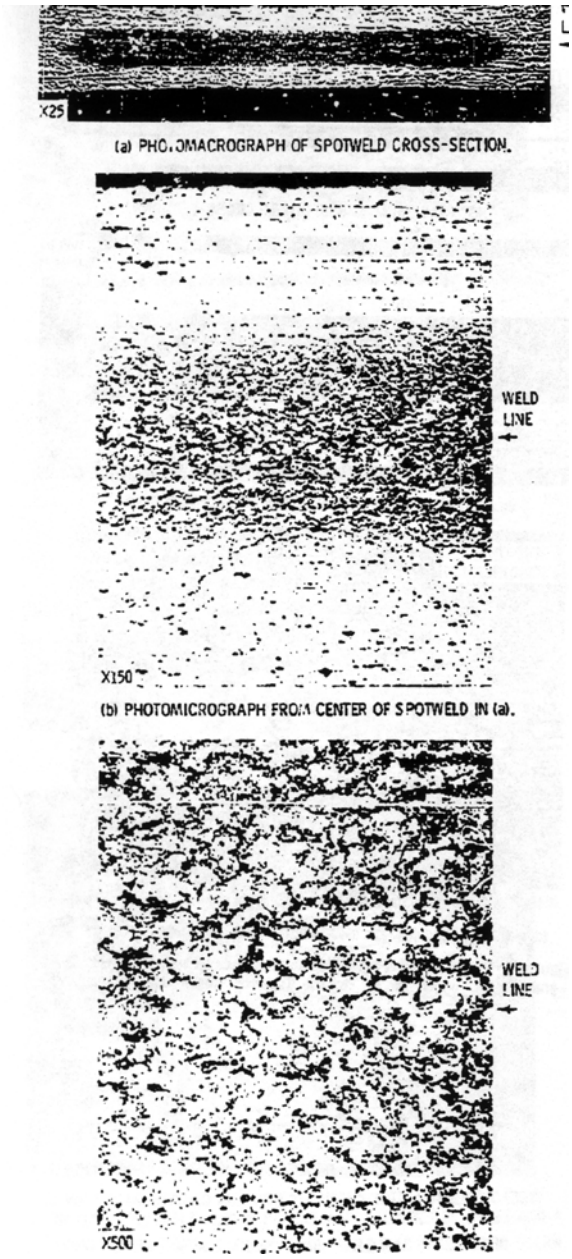

Fig. 16. Cross section of a fusion resistance spot weld made in TD-NiCr sheet using reduced power: (a) macro view of the spot-welded cross section (electrolytically etched at 3v DC in 100 ml H_2O, 2 g Cr_2O_3, 10 ml H_2SO_4); (b) micrograph from the center of the spot weld shown in (a); and (c) and higher magnification view from the center of (b) (after Holko et al.[7]).

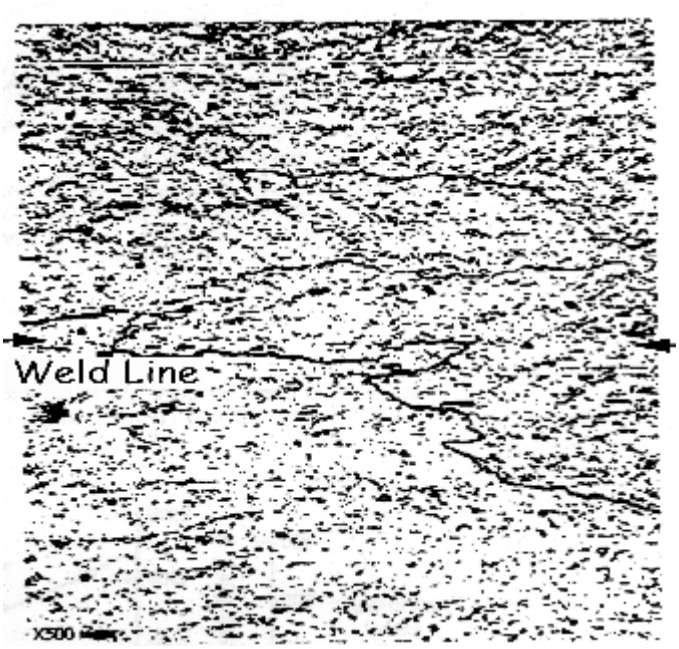

Fig. 17. Cross section of a solid-state resistance spot weld made in specially-processed TD-NiCr sheet and subsequently recrystallized (electrolytically etched at 3v DC in 100 ml H_2O, 2 g Cr_2O_3, 10 ml H_2SO_4) (after Holko et al.[7]).

In Fig. 18 the tensile shear strengths of TD-NiCr sheet spot welded using fusion and solid state processes are compared as a function of sheet thickness in tests run at room temperature and 1090°C. At room temperature, 'button pull-out' failures commonly occurred at the edge of the spot-weld and through the parent metal, and the shear strengths (for both welding processes) depended roughly on the sheet thickness. At 1090°C (and 1200°C), the spot-weld shear strength appeared independent of sheet thickness, and both 'button pull-out' and failure through the weld occurred regardless of strength. Holko et al.[7] pointed out that the solid state spot welds used in the tests were not made under optimum conditions, and that most exhibited a small-grained microstructure at the weld interface. Further, variations in the quality of the TD-NiCr sheet were thought to have contributed to the scatter in the data; the manufacturing process for the sheet had not been standardized at the time of the testing.

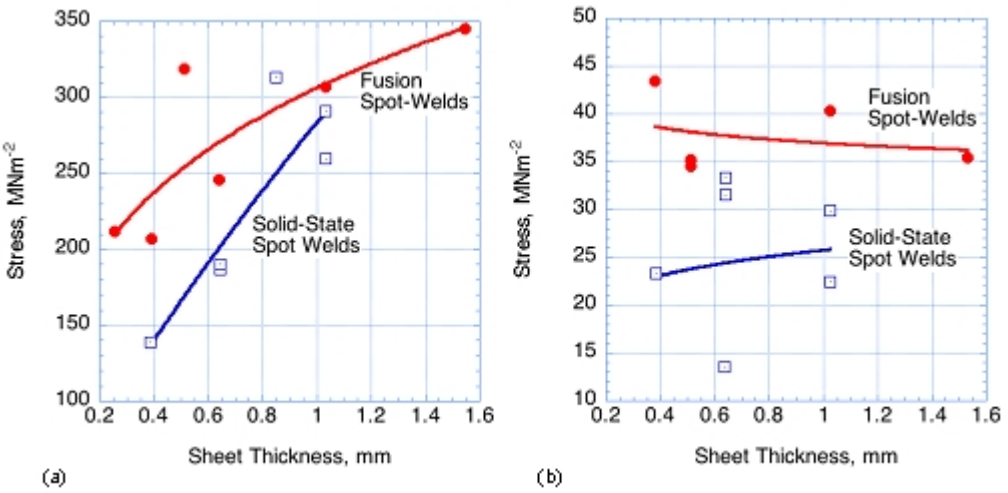

Fig. 18. Tensile shear strength at RT and 1090°C of spot-welded T-NiCr sheet, as summarized by Holko et al.[7]; (a) tested at room temperature; (b) tested at 1090°C.

Figure 19 summarizes typical creep-rupture shear strengths for TD-NiCr sheet spot welded using both fusion and solid-state processes.[8] Failure shear loads were included in the plot to allow comparisons with rivets and 'load-per-spot' data for other materials. The higher shear loads exhibited by the solid-state spot welded joints resulted from the larger diameter, hence larger area, than the fusion spot welds. 100-h creep strength data from several other authors also were summarized by Holko et al.[7] and are shown in Table 11. Failure in those welds was generally through the spot weld. TD-NiCr appeared to be stronger than the spot welds in 1 mm sheet, but there was scatter in the data since some specimens of both fusion and solid-state spot welds failed on loading at stresses similar to the 100-h creep-rupture shear stress.

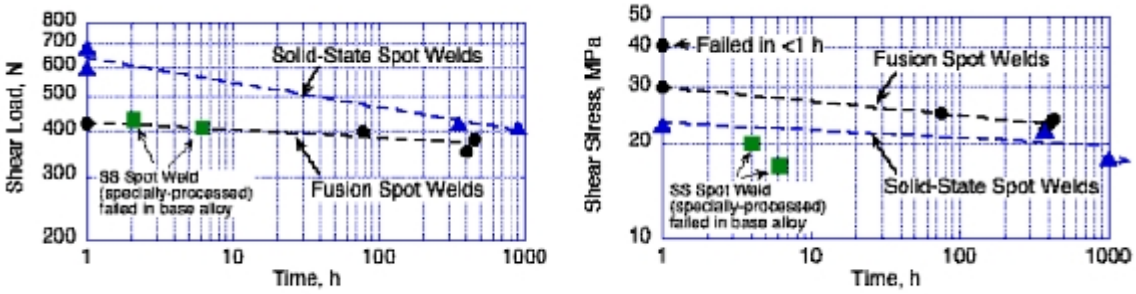

Fig. 19. Comparison of creep-rupture shear strengths at 1090°C of joints made in TD-NiCr sheet by fusion and solid-state spot welding (as summarized by Holko et al.[7]).

The room-temperature fatigue strengths of joints made in 0.4 mm thick and 0.5 mm thick TD-NiCr sheet using both fusion and solid-state single-spot welding (Figs. 20 and 21, respectively), were very similar. For the 0.5 mm sheet, the solid-state welds were slightly stronger, probably due to the larger spot diameter: 5.5 vs 4.3 mm (see Table 10). Nevertheless, these fatigue failure loads are low compared room-temperature failure loads (445 N vs 4kN; Table 10). However, since these values were for single-spot welds, multiple-spot welding would probably be a practical option, and strength measurements for joints should be obtained before spot welding is ruling out for a particular application.

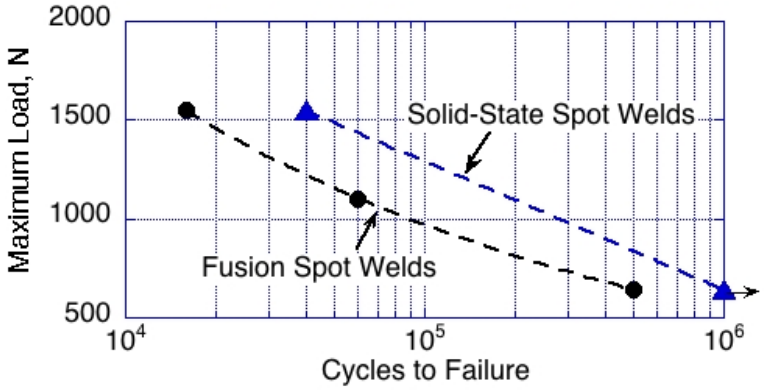

Fig. 20. Room-temperature fatigue strength of joints made in 0.4 mm thick TD-NiCr sheet using single-spot spot welds (as summarized by Holko et al.[7]).

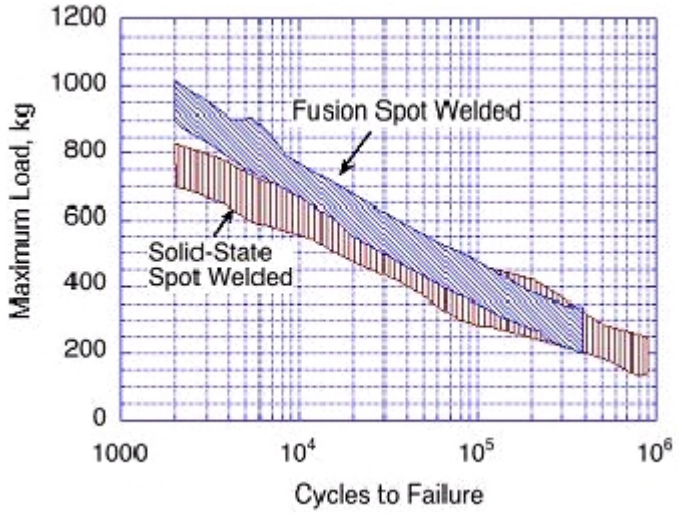

Fig. 21. Room-temperature fatigue strength of joints made in 05 mm thick TD-NiCr sheet using single-spot spot welds (as summarized by Holko et al.[7]).

7.6 RESISTANCE SEAM WELDING

Holko et al.[7] reported the results of trials to use resistance seam welding to fabricate a corrugation-stiffened heat shield panel from TD-NiCr sheet. The heat shield design involved a lap joint between a 0.25 mm-thick corrugation and a 0.4 mm-thick face plate. For this application, refractory metal wheel electrodes were used (instead of Cu electrodes) to heat the entire thickness of the TD-NiCr sheet to just below its melting point in an inert atmosphere. However, excessive distortion occurred in the region of localized heating. Nevertheless, further development of this process led to some success, and the ability[33] to produce sound, solid-state seam welds free from unwelded areas or cracks. Failure in tensile-shear testing typically occurred in the parent metal for 5t overlaps. Some panel warping persisted.

8. ELECTRO-SPARK DISCHARGE

8.1 PROCESS DESCRIPTION

The electro-spark discharge (ESD) process is a capacitor discharge, micro-arc welding process that uses short-duration electrical pulses that are discharged at controlled energy levels. Using a moving electrode in contact with the substrate produces fine molten droplets that then cool at a rapid rate, so that the area being joined is modified to become a zone of redeposited splats that result in a metallurgical bond. The heat-affected zone is very small.[34]

8.2 APPLICATION TO ODS ALLOYS

This technique has characteristics that appear to fit with the requirements for ODS alloys for minimizing the area of microstructural disruption in the vicinity of the joint. Miao et al.[34] used an ESD unit manufactured by Advanced Surfaces and Processes, Inc. (Cornelius, Oregon) to make butt welds in specimens 10 x 17 x 2 mm taken from 25 mm diam. bars of alloy MA957. The electrode was ground from the MA957 stock, and a pulse rate of 400 Hz was used at 150V. The surfaces to be joined were ground to a radius of approximately half the thickness, and then joined in air by filling with ESD deposit, one side at a time.

Figure 22(a) illustrates the layered structure typical of an ESD joint, while Fig. 22(b) shows that considerable porosity was present. Such porosity was considered to be unacceptable in terms of joint strength, although it was expected that it could be substantially reduced by simple process modifications;[26] the main concern of this particular study was the extent to which the dispersoid (especially nano-scale clusters of T-Y-O, or NF) had undergone dissolution or coarsening. Examination by transmission electron microscopy and small angle neutron scattering indicated a significant increase in size, and a reduction in number density and volume fraction of the NF. The results of a room-temperature tensile test on a single ESD joint indicated that the tensile strength (UTS) of the joint was approximately 63% of that of the monolithic alloy (656 vs. 1035 MPa).

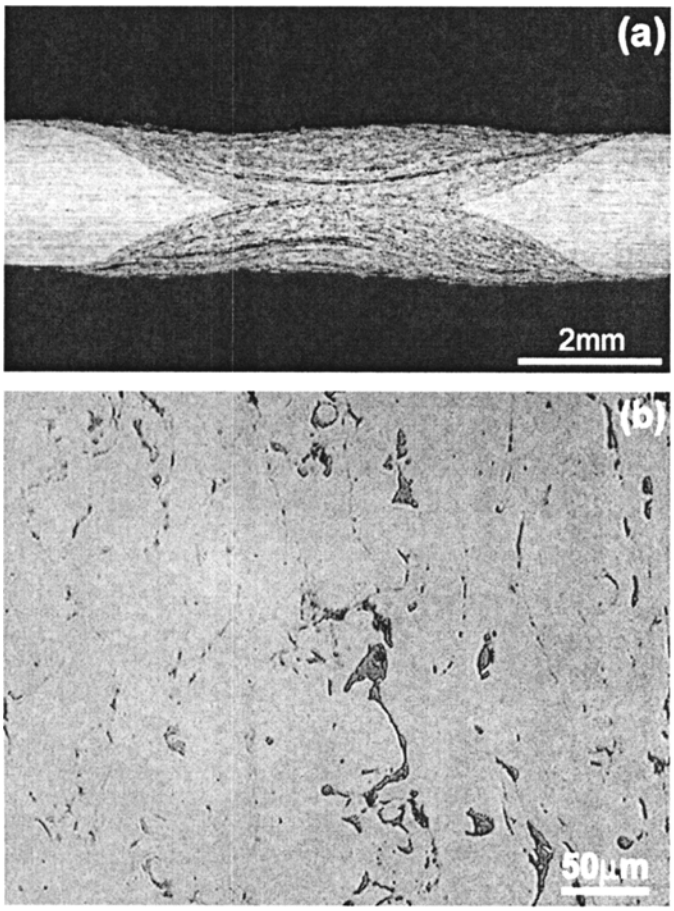

Fig. 22. Cross sectional views of a joint made in MA957 by ESD; (a) complete joint; and (b) example of the porosity present in the joint (unetched) (after P. Miao, et al.[34]).

9. EXPLOSIVE BONDING

9.1 PROCESS DESCRIPTION

Explosive bonding is a solid-state joining process in which an explosive charge provides the driving force to accelerate the parts to be joined so that they collide at high speed and pressure in a controlled manner and with the requisite energy to produce plastic flow and a metallurgical bond. Bonding occurs with minimum heat input and no heat-affected zone is formed. The process requires that the parts to be joined are positioned with a precisely-controlled stand-off distance and relative angle to each other. The explosive force brings the two components together in a collision front that advances progressively; the rate of advancement of the front must be slower than the speed of sound in both materials to avoid interference from shock waves. A jet of metal is expelled just ahead of the collision front, and strips oxides and contaminants from the surface, ensuring a clean interface for bonding. The resulting bond has a characteristic, directional wavy appearance in cross section. Figure 23 shows schematically how the process progresses.[30] The use of explosive bonding in commercial applications began in the 1950's,[35] and a signal application was the production of clad coinage for the US Mint.

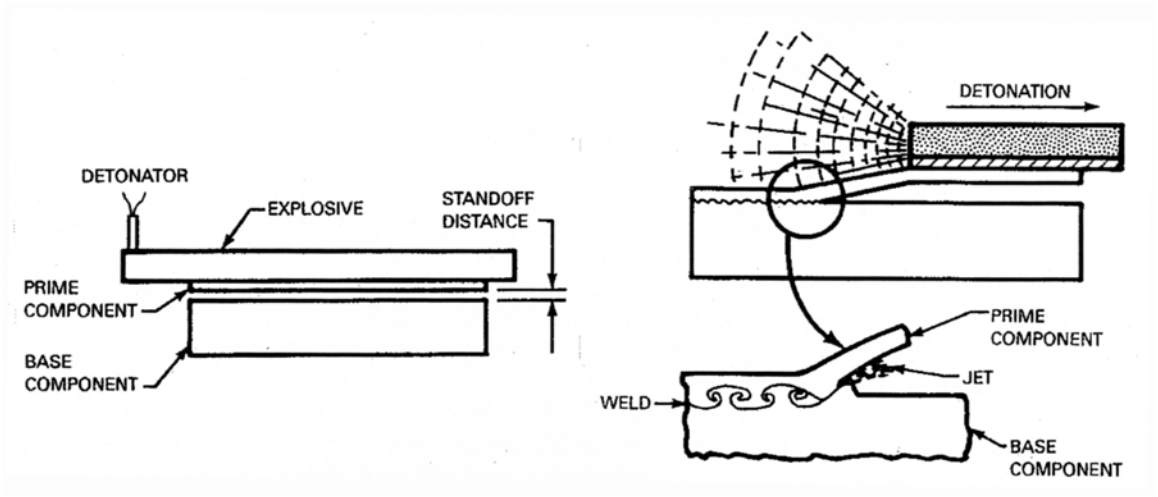

Fig. 23. Schematic depiction of stages in the explosive bonding process (after L. E. Brown et al.[30]).

9.2 APPLICATION TO ODS ALLOYS

In commenting on the experience of explosive bonding of TD-NiCr sheet by the General Electric Company under a US Air Force Materials Laboratory contract, Holko et al.[7] noted that tensile-shear properties similar to those of brazed joints were obtained. The lower than anticipated strength of the joints was attributed to the formation along the weld line of a band of small, recrystallized grains during the post-weld heat treatment of 15 min. at 1300°C. The base metal was heavily worked during the explosive bonding, and also recrystallized after the heat treatment. It was recommended that the extent of cold working in the base metal and at the interface be minimized to avoid such recrystallization.

The high-temperature strength of explosively-welded lap joints in MA956 were reportedly close to that of the parent metal. Crack-free joints typically require the alloy to be heated above the brittle-to-ductile transition temperature, and slowly cooled after joining.[36]

The fabrication of an ODS heat exchanger capable of producing air at 1100°C was undertaken in a European COST 501 program led by British Gas.[37] Tubes of alloy ODM751 (3600 mm long; outside diameter 27 mm; and wall thickness of 2.9 mm) were explosively bonded to the insides of thick-walled stubs of spun-cast stainless steel CR39W (35Ni-25Cr-1Nb-1Mn-0.1C), which were then joined into the header by conventional fusion welding. Figure 24 is a schematic representation of such a joint. The harp-design, 34-tube heat exchanger was run successfully with radiant tube temperatures up to 1150°C at 3.5 barA; no joint problems were reported.[38]

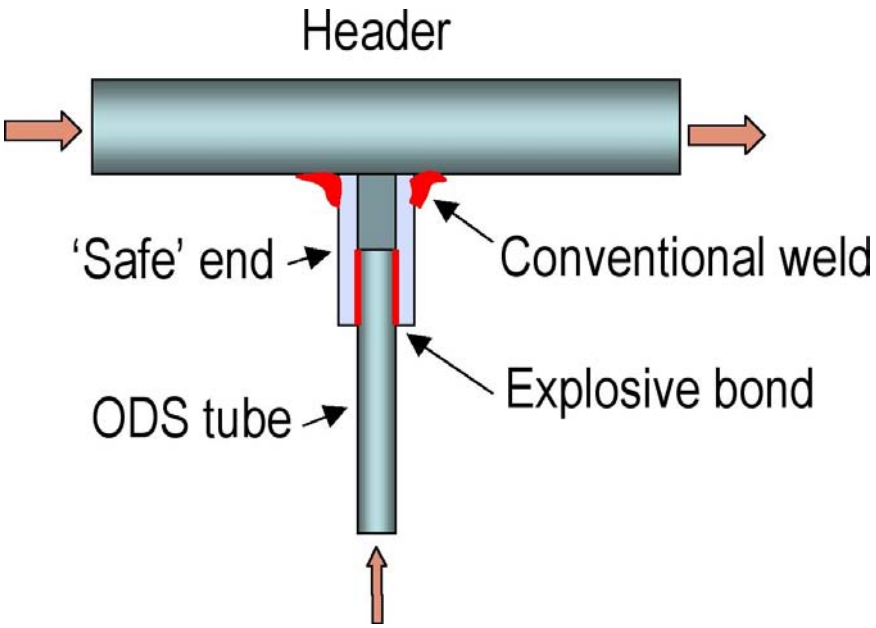

Fig. 24. Schematic representation of the joint configuration used in European COST Action 501.

Brown et al.[30] used explosive bonding to join plates of MA956, and to join MA956 and Inconel 601; in the latter case the MA956 was accelerated into a stationary Inconel 601 plate. Samples of dimensions 102 x 152 x 6.35 mm were used. The interfaces between the bonded MA956-MA956 and MA956-Inconel 601 plates after a post-welding heat treatment of 1 h at 1000°C are shown in Fig. 25, and exhibit the wave-shaped features characteristic of a successful joint. Shear strengths measured at room temperature for as-welded and post-weld heat-treated conditions, listed in Table 12, indicate a slight decrease following heat treatment of the MA956. The increase in strength of the MA956-Inconel 601 joint following heat treatment was ascribed to the relatively high ductility of the annealed Inconel 601.[30]

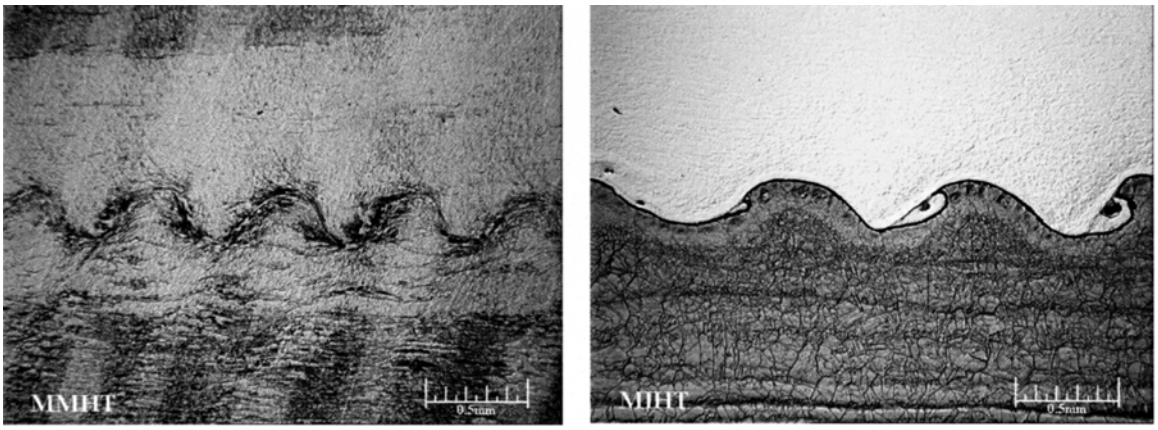

(a) (b)

Fig. 25. Optical micrographs of cross sections of explosively-bonded plates (a) MA956-MA956; and (b) MA956-Inconel 601 (after L. E. Brown et al.[30]).

Table 12. Room-temperature shear strengths of explosively-bonded plates of MA956[30]

Material	Shear strength (MPa)
MA956-MA956 (as joined)	565.4
MA956-Inconel 601 (as joined)	548.1
MA956-MA956 (PWHT of 1000°C for 1 hr)	532.3
MA956-Inconel 601 (PWHT of 1000°C for 1 hr)	611.6

10. FRICTION/FRICTION-STIR WELDING

10.1 PROCESS DESCRIPTION

Friction welding is a process for joining metals without fusion or filler materials, and involves rotating one component at high speed against another to generate heat.[39] The force applied to form the joint varies with the application, but typically is relatively low unless some level of forging is desired. There are several variants of friction welding; while it is usual for at least one of the components to rotate, a method of butt welding of plates by linear friction welding also is available. Size restrictions are related to the capacity of the equipment to generate sufficient torque.

10.2 INERTIA-DRIVEN FRICTION WELDING

In this version of friction welding, one component is held in a collett device on a rotatable spindle attached to a flywheel of a specific weight. The other component is held in a non-rotatable, chucking device on the tail stock. The welding cycle consists of accelerating the spindle to a pre-determined and set speed (based on energy input requirements). At the predetermined flywheel speed, the drive is disconnected, allowing the mass of the rotating components to be free and driven solely by their kinetic energy. At the same instant, a controlled, axial pressure is applied to force the components to be joined together, causing the energy of the rotating mass to be dissipated by friction at the weld interface. This pressure or “load” is maintained until all of the energy in the rotating mass has been consumed in the weld, and the rotating component has stopped. During the welding cycle, the metal interfaces are hot worked together as a result of the frictional heat, and some material is forged out of the weld. This results in some length loss, or “upset.” Because of the inherent repeatability of the energy input under controlled pressure, the amount of upset is very reproducible for a given material/component configuration, and is a key initial factor in monitoring/determining weld quality.

10.3 APPLICATION TO ODS ALLOYS

Systematic examination of the effect of some processing parameters on the inertia friction-welding of fine-grained MA956 tubes indicated that lower force levels and higher surface velocities in the friction and upset phases of the process resulted in the expelled material (‘flash’) having characteristics that suggested that molten alloy had been present during the welding.[30] Formation of liquid during welding of ODS alloyswould likely result in agglomeration of the oxide dispersoid particles, and was thought to have promoted the observed grain growth. The flash was associated with the presence of a large alloy grain size in the worked area. Increasing the welding force to close to the yield strength of the alloy at 871°C, using a single-stage thrust load, and decreasing the surface velocity to reduce the peak temperature resulted in a clean-appearing bond line and a finer alloy grain size, as illustrated in Fig. 26. Three distinct regions were defined in the weld structure: (a) a central region with coarsened grains; (b) a recrystallized, fine-grained region; and (c) the forged region with large changes in the directions of the elongated grains. It was also considered likely that the fine, elongated grains in the high thrust load/low surface velocity welds retained a high level of strain, which could promote the formation of a large alloy grain size in the bond region upon subsequent recrystallization heat treatment.

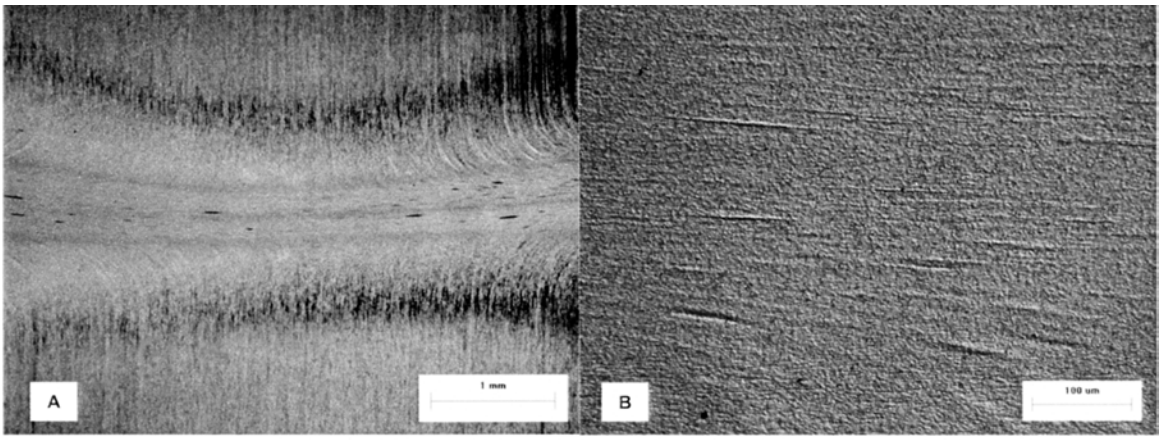

Fig. 26. Cross section of a weld produced in fine-grained MA956 by high thrust-load inertia friction welding, showing (a) the macro appearance of the joint, and (b) the fine alloy grain size in the joint.[30]

Inertia friction welds also were made between tubing of MA956 and Inconel 601.[30] It was found necessary to reduce the thrust load (compared to that used for MA956-MA956 joints) to avoid bending of the Inconel 601 tubing. Table 13 summarizes the optimized welding parameters resulting from this study.

Table 13. Optimized processing parameters for inertia friction welding of MA956[30]

Materials	Inertia (wK^2)	Spool speed (rpm)	Thrust load (kg)	Loss of length (mm)	Flash curl
MA956 (fine-grained)	900	605	34, 019	12.2	Smooth, thin
MA956[a]	900	600	34, 019	12.1	Smooth, thin
MA956[a] to Inconel 601	900	570	30390	10.7	Smooth, medium thickness

[a]Recrystallized

Kad et al.[3] used inertia friction welding to make butt joints in 6 cm OD x 5 mm wall, unrecrystallized MA956 tubes, as indicated in the sequential photographs in Fig. 27. As anticipated, there was massive deformation of the alloy microstructure in the immediate vicinity of the joint (Fig. 28). However, this deformation was very localized, with a sharp demarcation visible with the original alloy microstructure (shown after recrystallization of the joined alloy), which clearly indicated that the large grains followed the axial direction of the

tube to the boundary with the deformed material, at which point they followed the flow path of the deformed material in the joint. Because of the variation in alloy microstructure through the wall thickness of the alloy in the vicinity of the joint, the mechanical properties of the joint (in creep) are expected to vary with location through the joint. Creep testing of specimens extracted from locations where obvious differences in microstructure prevailed was in progress at the time of reporting.[3] Note also that the joining parameters used were far from being optimized for this alloy; the results of these analyses were to be used to iterate those parameters in search of maximum joint creep strength.

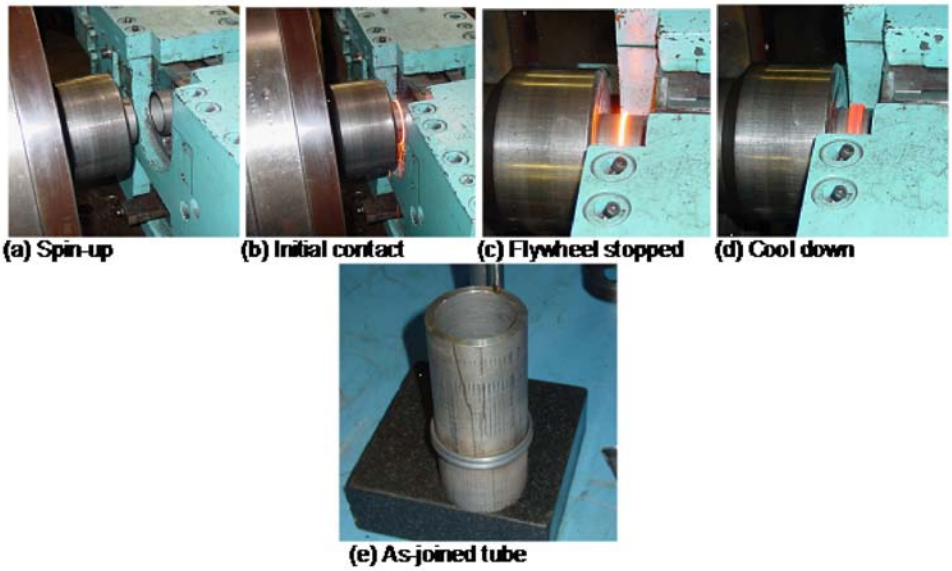

Fig. 27. Sequences in the inertia welding of a MA956 Tube (after B. K. Kad et al.[3]).

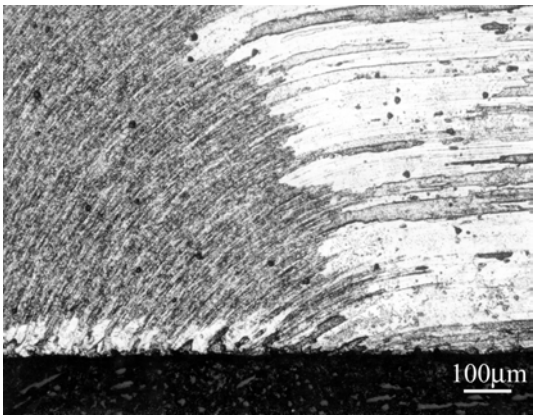

Fig. 28. Cross section of a joint formed in MA956 by inertia welding, showing the extent of microstructural deformation (after B. K. Kad et al.[3]).

This technique appears to have promise for producing components such as end caps of flanges on tubes or pipes made from ODS alloys. Figure 29 illustrates schematically the configuration of a joint associated with such a component.

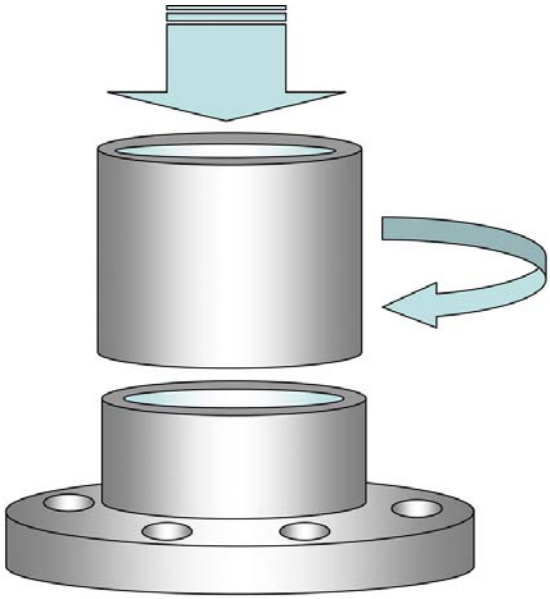

Fig. 29. Schematic representation of the use of friction welding to fabricate flanges from ODS alloys.

10.3 FRICTION-STIR WELDING

This is a variant of friction welding (invented by TWI, Cambridge)[40] in which the component parts to be joined are stationary, and the weld is created by the combined action of frictional heating and mechanical deformation due to a rotating tool. As a result, this process is most suited to flat, long components (plates and sheets), but can be adapted for pipes, hollow sections and positional welding. The maximum temperature reached is of the order of 0.8 of the melting temperature of the work piece. The tool has a circular section except at the contact end (pin or probe), which is given a specific shape that often is job-specific.[41] For friction stir-welding of low melting-point alloys (such as Al), the probe is made of a suitably hardened steel, whereas for alloys with higher melting points, the probe also requires a higher melting point, and refractory metals such as W may be used.

The probe penetrates the work piece so that the junction between the cylindrical portion of the tool and the probe end (shoulder) rubs on the top surface of the work piece, generating heat primarily by friction. There is also a volumetric contribution to heat generation from the adiabatic heating due to deformation near the probe tip. Since this induced heating decreases as the work piece becomes thicker and the ratio of frictional-to-volumetric deformation changes, the welding parameters must be adjusted accordingly to ensure sufficient heat input per unit length.

The microstructure of a friction-stir weld depends on a number of parameters: the tool design; the rotational and translational speeds of the tool; the applied pressure; and the characteristics of the material(s) being joined. A heat-affected zone (HAZ) is formed as in conventional welds, the width and shape of which (as well as the average grain size in the HAZ), being influenced by the temperature developed in the joining process.[42] The structure of a joint made by friction-stir welding is conventionally described in terms of the major zones observed:[43] a thermomechanically-affected zone; a central region (or 'nugget') containing a layered 'onion-ring' flow-pattern; and a 'stir zone.' This latter is the most severely-deformed region, and often results in dynamic recrystallization and the formation of a fine, equiaxed grain structure. The onion-ring structure results from the tendency of a threaded tool to transfer material from the front to the back of the weld via the extrusion of cylindrical sheets of material during each rotation of the tool. The grain structure of the thermomechanically-affected zone is essentially a deformed version of the original alloy microstructure; also, there is a gradation in microstructure across the alloy that results from the shearing action induced by the shoulder of the rotating tool.

10.4 APPLICATION TO ODS ALLOYS

Since no melting is involved, friction welding would not be expected to result in excessive agglomeration of the oxide dispersoid.[13] Nevertheless, the significant work imparted in the immediate vicinity of the joined interfaces is sufficient to provide the driving force for local recrystallization of the alloy during post-joining heat treatment. A further consideration is that the working of the alloy near the joint has a distinct directionality from the rotating tool, and this influences the orientation of the large aspect-ratio grains formed upon secondary recrystallization. Also, in the region of maximum work input, the formation of fine, essentially equi-axed grains is promoted, resulting in a gradation in grain size and directionality in grain structure of the alloy around the joint.[29,44,45] Several authors have reported some modification of the size and shape (and composition) of the oxide dispersoids at the joint in MA956 and ODS FeAl].[46] Thus, it is to be expected that the creep properties in the region of the bond line will be different (typically lower) from those of the monolithic, recrystallized alloy. High forging pressures and low welding times appeared to beneficially influence the tensile strength of friction-welded MA956.[29,47,48]

There are several reports of the successful friction welding of alloy MA956 to itself.[45,47] Also, rotary friction welding has been used to demonstrate the ability to join rods of ODS-Fe_3Al to wrought Ni-base alloys (in both cold-worked or annealed conditions).[47] Harper[48] described the friction welding of MA956 tubing to Inconel 601 (hot finished bar, solution annealed at 1093°C); the resulting room-temperature mechanical properties were considered to be very promising, and are listed in Table 14.

Table 14. Typical properties for joints between MA956 and Inconel[48]

Alloys	Ultimate tensile strength (ksi)	Yield strength (ksi)	Elongation (%)
MA956	86	70	9
MA956/601-1	39.6	37.6	<1
MA956/601-2	26.4	19.8	<1
MA956/601-3	43.2	42.4	<1
MA956/601-4	40.5	40.3	<1
Inconel 601	107.5	42.1	47

Feng and Ren[49] reported that both lap joints and butt joints can be made successfully in 1.2 mm-thick recrystallized (large-grained) MA956 sheet by friction-stir welding. The materials to be joined were first polished with 600 grit abrasive paper (to remove the surface oxide scales), and then degreased with ethanol. Typical welding conditions were 1000 rpm, 25 mm/min travel speed tool using a 12 mm diameter tool made of a SiO_2-based ceramic. A TP304 stainless steel backing plate was used to support the sheets being joined. In the butt weld, two microstructurally-distinct regions were identified in these welds (see Fig. 30): a wide zone with equiaxed, recrystallized grains approximately 20-40 μm in size ('stir zone'), and a thin, severely-deformed surface layer that exhibited grains sizes in the range 5-10 μm. The transition from the stir zone to the parent metal was very sharply defined. Only partial bonding was achieved in the lap joint (Fig. 31). Transmission-electron microscopy revealed that, in the stir zone of the butt weld, high-angle grain boundaries predominated, and the grains were relatively free of dislocations, suggesting that dynamic recrystallization occurred in this region. Also, while a limited amount of coarsening of the oxide dispersion was observed, a large population of such particles was retained in the grains, suggesting that the weld may retain good high-temperature creep strength. No mechanical properties were measured for the joints, but it was noted that there was a slight decrease in the hardness of the stir zone.

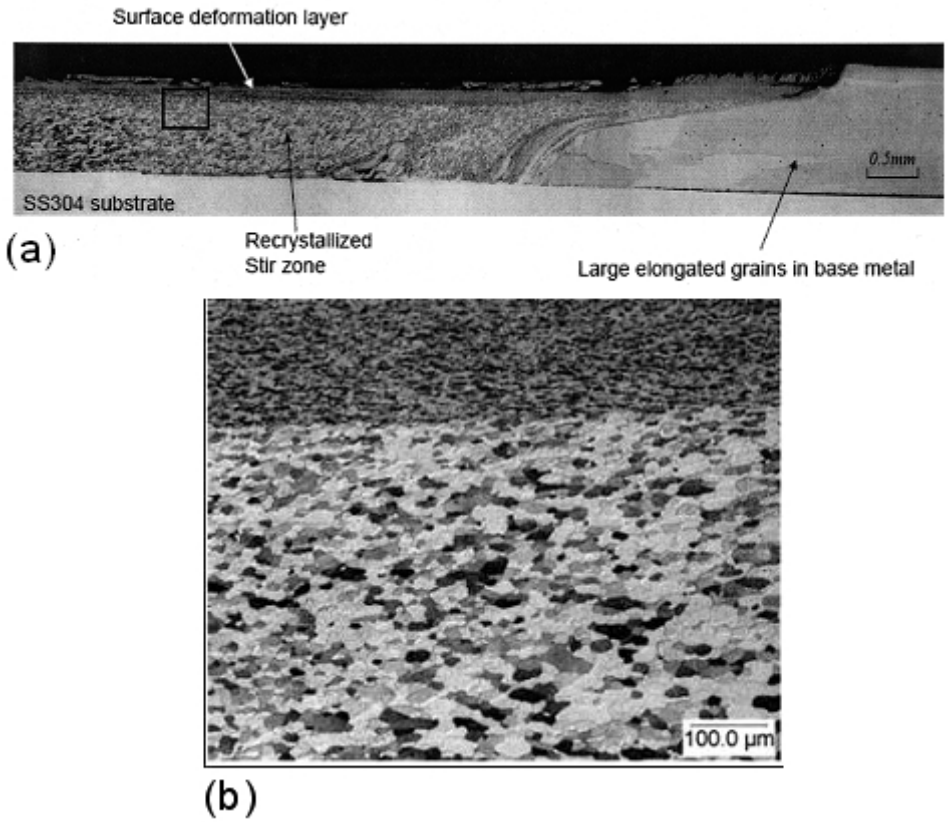

Fig. 30. Cross sections of a butt joint in MA956 made by friction-stir welding showing (a) macro view of the joint; and (b) micro-structure of the stir zone from the rectangle in Fig. 28(a) (after S. Kallee et al.[39]).

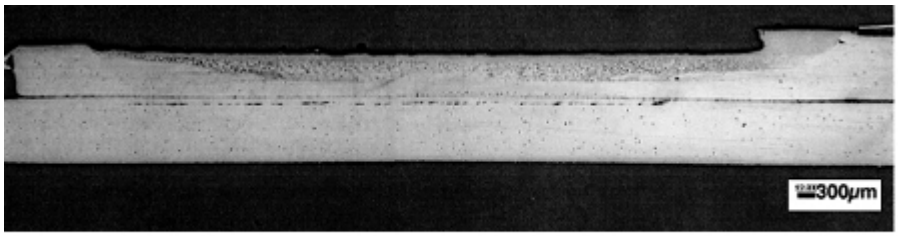

(a)

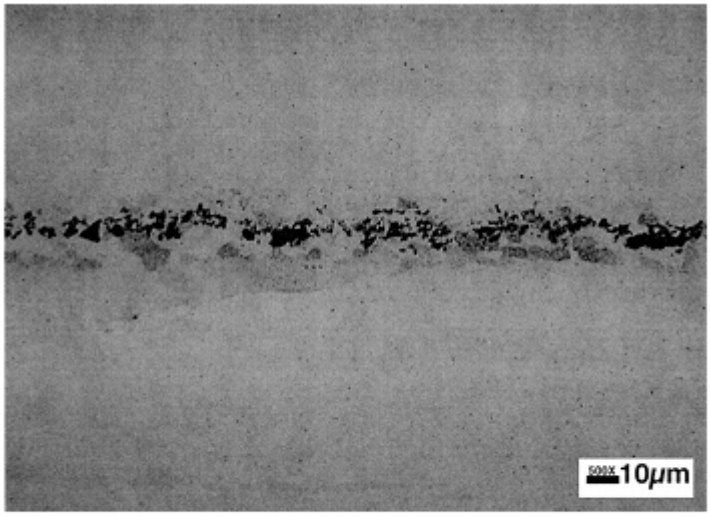

(b)

Fig. 31. Cross sections of a lap joint in MA956 made by friction-stir welding showing (a) macro view of the joint; and (b) higher magnification view showing porosity along the bond line (after Z. Feng, et al.[49]).

11. MAGNETIC IMPULSE WELDING

11.1 PROCESS DESCRIPTION

This welding process was developed in Russia in the late 1960s/early 1970s for welding the end closures of nuclear fuel rods, and was described in U.S. patent #4,150,274 issued to three Russians in 1979. Maxwell Laboratories, Inc.[32,50] licensed the technology and built welding equipment for Westinghouse Hanford Co., for use in nuclear fuel manufacturing for the U.S. Department of Energy. Other companies involved in the early development of pulsed magnetic welding in the United States included Douglas United Nuclear, Inc. (Richland, WA) and General Atomic Technologies Corp. (San Diego, CA).

In this process, a magnetic field is used to rapidly collapse one component onto another, forming a metallurgical bond. The parts to be welded are oriented coaxially (the outer piece must be a good electrical conductor) and are placed into a specially-designed coil. Energy stored in a capacitor bank is discharged into the coil, creating two magnetic fields, one in the coil, the other created by the induced current in the outer part to be welded. The magnetic field in the outer work piece opposes that in the coil, creating a repulsive force that drives the outer work piece and the stationary, inner work piece together at an extremely high rate (achieving speeds >300 m/s), creating a solid-state weld. The actual process occurs in microseconds, and the welding cycle occupies approximately one second. Key issues are the design of the tooling to control the component orientation, and of the coil (which must withstand the force used to drive the materials together).

One caveat is that the parts being joined must have a closed section, so that eddy currents can circulate and create the opposing magnetic fields. Also, the higher the conductivity of the work piece, the more efficient the system. While the process is most readily applied to joining two cylindrical components, where one is collapsed onto the other, research is in progress to design a coil for applying this process to flat sheets.

11.2 APPLICATION TO ODS ALLOYS

Since bonding occurs at a significantly lower temperature than with traditional welding, this process is well-suited for joining dissimilar metals. This technique has long been used on ferritic (HT9) tubing. In tests by Pacific Northwest Laboratory,[10] sufficient progress was made to demonstrate the feasibility of using this technique for welding end caps of HT9 on to tubing of MA956 and MA957. However, only one parameter—voltage—was varied. The MA956 samples were machined from 12.45 mm diam. bar stock provided by INCO. The samples of MA957 were developmental tubes fabricated by the Superior Tube Company using inter-pass anneals at 900 or 1000°C.

Higher quality bonds were achieved with end cap designs which had a single taper (10°) or a double-angled (8/12°) taper in the plug, than one with a single taper of 7°, which led to gross cracking in the end plug. Higher energy levels were needed to produce successful welds in the ODS alloys compared to HT9 or austenitic steels. Nevertheless, some centreline cracking occurred in the HT9 end plug, particularly at higher energy input levels. The oxide on the surface to be joined was removed with 600 grit (U.S.) paper.

Good bonds were reported using 9.5 and 19 mm-long driver sleeves that had a wall thickness of 0.53 mm. Thinner sleeves (0.38 mm) produced unsatisfactory welds, while thicker sleeves (0.635 mm) exhibited incipient melting at the sleeve end. Examples of the microstructures of welds in MA956 and MA957 are shown in Fig. 32. The results from welding tests are summarized in Tables 15 and 16. The rippled interface expected from this technique, indicating intimate metallurgical contact, is clearly visible for both alloys.

(a) (b)

Fig. 32. Micrographs of sound welds in (a) MA956; and (b) MA957 (after Data source[5]) (magnification provided in the original report).

Table 15. Results from pulsed magnetic impulse-welding feasibility studies[10]

Sample No.	Prior heat treatment	kV	He leak test	Bond length		Metallography
				Axial (mm)	Circumf. (°)	
MA956						
16307	None	35.0	—	1.0-1.8	360	Solid state weld, no cracks
16308	None	35.0	—	0-1.3	220	Solid state weld, no cracks
MA957						
16586	1000°C	35.0	—	None	None	—
16592	1000°C	35.0	Leak	0.5-1.0	150	—
16603	1000°C	36.0	No leak	0.5-2.5	360	Solid state weld, no cracks
16614	900°C	36.0	No leak	0.5-1.3	360	Solid state weld, no cracks
16615	900°C	37	No leak	1.3-2.5	360	Solid state weld, no cracks

Table 16. Average hardness in magnetic impulsed-welded samples[10]

Sample No.	Prior heat treatment	Microhardness (DPH; 500 g load)			
		HT9 End Cap	Approx. 7.6 mm from weld	Adjacent to weld	ODS/HT9 weld interface
MA956					
16308	None	272	327	358	348[a]
MA957					
16603	1000°C	284	407	407	323
16615	1000°C	274	427	428	359

[a]Single hardness value; others were average of 2 and 3 values.

Brown et al.[30] conducted trials with 12.7 mm diameter tubes of MA956, using a lap configuration (Fig. 33) and a Cu sleeve to aid in coupling the pulse energy to the components being joined. A 1/4t wall thickness (joint thickness 1/2t) was used initially to ensure success with the (relatively low-power) 90 kJ magnetic pulse system used. For welding MA956 to Inconel 601, the Inconel was made the outside tube. Successful joints were obtained, with an appearance in cross section similar to that of an explosively-bonded joint (Fig. 34). No mechanical property measurements were reported.

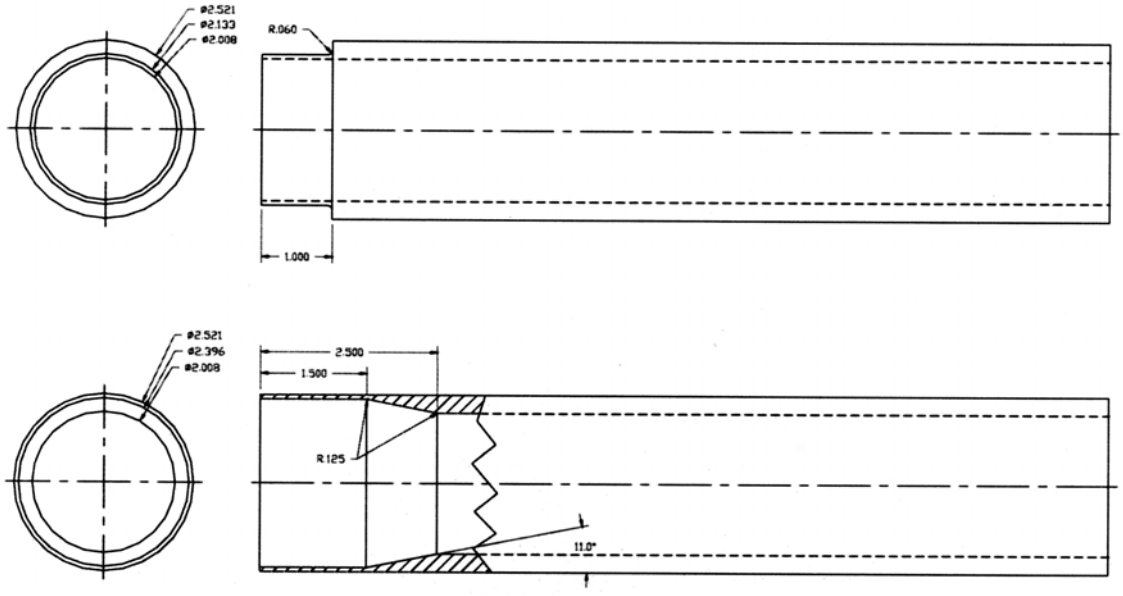

Fig. 33. Lap joint configuration used for magnetic impulse welding of MA956 tubes.[30]

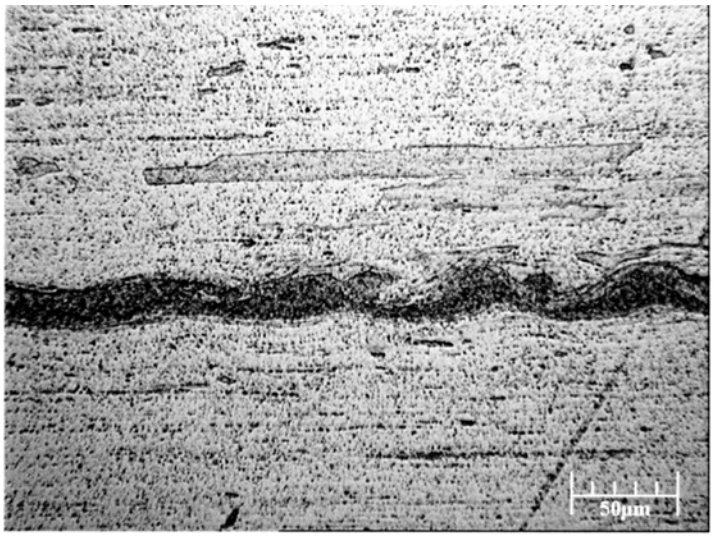

Fig. 34. Cross section of a joint in MA956 made by magnetic impulse welding.[30]

12. DIFFUSION BONDING

12.1 PROCESS DESCRIPTION

Diffusion bonding typically involves prolonged contact of the surfaces to be joined under controlled conditions of time, temperature, and pressure. Fixturing is an important consideration since the components being joined must be held in accurate register for the duration of the processing. Pressure may be applied uniaxially or isostatically. Where pressure is applied uniaxially, the nature of the fixturing typically dictates pressures that will not result in deformation of the work (usually in the range of 10-30 MPa). For hot, isostatic pressure joining, higher pressures can be applied, and deformation of the work may be included in the bonding process. The surfaces to be joined typically are required to have a fine surface finish, and to be scrupulously cleaned. However, if deformation is an intended contribution to the bonding process, some level of surface roughness may be advantageous.

12.2 APPLICATION TO ODS ALLOYS

Holko et al.[7] summarized the extensive work by NASA and contractors on the joining of TD-NiCr sheet by diffusion bonding. For commercial-grade sheet, temperatures in excess of 1190°C generally were used with various combinations of pressure and time; Table 17 indicates some of the conditions used. The overall experience was that the formation of a thin band of fine grains along the bond line, thought to result from recrystallization of locally-strained material (from belt-sanding of the surfaces prior to joining), apparently was unavoidable, and this feature lowered the creep strength of the welds. For such welds, fracture typically occurred along the weld line.

The use of a special surface preparation technique involving chemical or electrochemical polishing to remove the asperities and cold-worked layer resulting from surface sanding (mentioned earlier for solid-state spot welding, Section 7.5), allowed the formation of excellent bonds, and the ability for secondary recrystallization to proceed across the bond line. A two-step procedure was employed, in which the surface of unrecrystallized TD-NiCr was chemically or electrochemically polished, and diffusion bonded at a temperature below the secondary recrystallization temperature of the alloy (approx. 870°C), followed by secondary recrystallization. A 1.6 mm-thick TD-NiCr sheet that was diffusion bonded at 705°C and 210 MPa for 1 h, then recrystallized at 1190°C and 15 MPa for 2 h exhibited no residual bond line, and yielded creep rupture shear strength equal to that of the parent metal, with failure occurring away from the location of the bond line. Similarly-processed commercial (recrystallized) TD-NiCr sheet also exhibited parent metal strength, but retained a bond line, which typically was the site of failure. Test results are shown in Table 17. Further developments led to a single-step bonding process and a reduction in processing time.

Table 17. Summary of diffusion bonding parameters reported for TD-NiCr sheet (after Holko et al.[7])

Condition	Thickness (mm)	Joint configuration	Heat source	Joining parameters		
				T (°C)	Time (h)	Pressure (MPa)
Commercial grade	0.08	T-joint	Hot press	1315	1.5	2.7
	0.08			1200	11.5	2.7
	0.25		Resistance	1150	0	69
Recrystallized + specially processed	1.5	Lap joint	Hot press	705	1	210
Unrecrystallized + specialty processed	0.25			760	1+2	210+14

Further work by NASA demonstrated that diffusion bonding of the complex Ni-based ODS alloy MA6000 also is feasible.[51]

Hedrich et al.[14] emphasized the need for plastic deformation in the bonding zone in order to achieve sound joints. However, although the high strength of the ODS alloys requires that the applied pressures are very high, deformation from the application of excessively high pressures results in the formation of chains of porosity along the longitudinal grain boundaries. The result is that the range of applicable pressures is rather narrow; these researchers determined that plastic deformation of 0.2 to 0.4% was required, which translated to a load of 75 MPa for alloy PM2000, and 110 MPa for PM2010, at a bonding temperature of 1120°C. The surface preparation involved grinding, followed by degreasing and etching. Direct bonding produced very clean bonds; however, a degree of secondary recrystallization was observed in the bond, depending on the extent of micro-plastic deformation induced.

The application of this technique with a 50 µm-thick interlayer of Inconel 600 resulted in bonds with room-temperature bending strengths up to 70% of that of the parent alloy. A disadvantage of the use of such interlayers was that Kirkendall porosity developed from interdiffusion of Ni during the hat treatment. Nevertheless, bend rupture strengths up to 92% of that of the base alloy were measured.

Hedrich et al.[14] also demonstrated that bonding of fine-grained, unrecrystallized material with consecutive heat treatments allowed coarse grain growth across the bond. This required high local plastic deformation, but if local flow (plastic deformation >40%) occurred, the alloy did not form coarse grains, apparently due to loss of its 'texture memory.' Also, secondary recrystallization during direct bonding should be minimized. Bonding conditions involving approximately 10% plastic deformation, and bonding at temperatures below 1000°C to avoid recrystallization during bonding, were recommended. Optimized bonding parameters reportedly resulted in room temperature bending strengths of 75% of the base alloy.

Krishnardula et al.[31] examined diffusion bonding parameters for both MA956 and PM2000 in both the unrecrystallized (fine-grained) and secondary-recrystallized (large, elongated grained) conditions. The as-received, fine-grained MA956 was in the form of square-section bar (approximately 11 mm on a side), whereas the recrystallized alloy was a bar approx. 20 mm on a side; the fine-grained PM2000 was supplied as 25 and 50 mm diam. rods. The samples to be joined were in the form of specimens 11 x 10 x 2 mm cut by electric discharge machining. The mating surfaces were surface ground to ensure that they were flat and parallel (surface roughness of approx. 1 μm), degreased, and stored in acetone before use.

Initial bonding used a Gleeble 1500 thermomechanical cycling system (direct resistance heating) to provide rapid heating (8-10°C/s). A load was applied through Inconel 601 blocks. The trials also included a radiantly-heated vacuum furnace (with a lower heating rate of 2°C/s), and post-bonding heat treatment (PBHT) using a radiantly-heated furnace. In both cases, the heating rates employed were significantly faster that the capability of a typical commercial vacuum brazing furnace. In the radiantly-heated furnace, only a fixturing load was applied.

Several orientations of the blocks to be joined (as shown in Fig. 35) were used to vary the number of grain boundaries in the surfaces to be bonded. Bonding of the two versions of MA956 was attempted in the transverse-transverse (fine grain-fine grain), longitudinal-transverse (coarse grain-fine grain), and longitudinal-longitudinal (coarse grain-coarse grain) orientations at 1250°C for up to 10 min, followed by a post-bonding heat treatment (PBHT) of 1h at 1300°C. However, bonding occurred only when fine-grained surfaces were involved, as shown in Fig. 36; with the large grain-large grain orientation large unbonded areas were observed. This difference was thought to be due to the difficulty in deforming the large-grained (high-strength-condition) substrates to provide sufficiently intimate contact of the surfaces to be bonded, or possibly to the high-level of stored energy in the unrecrystallized substrates.

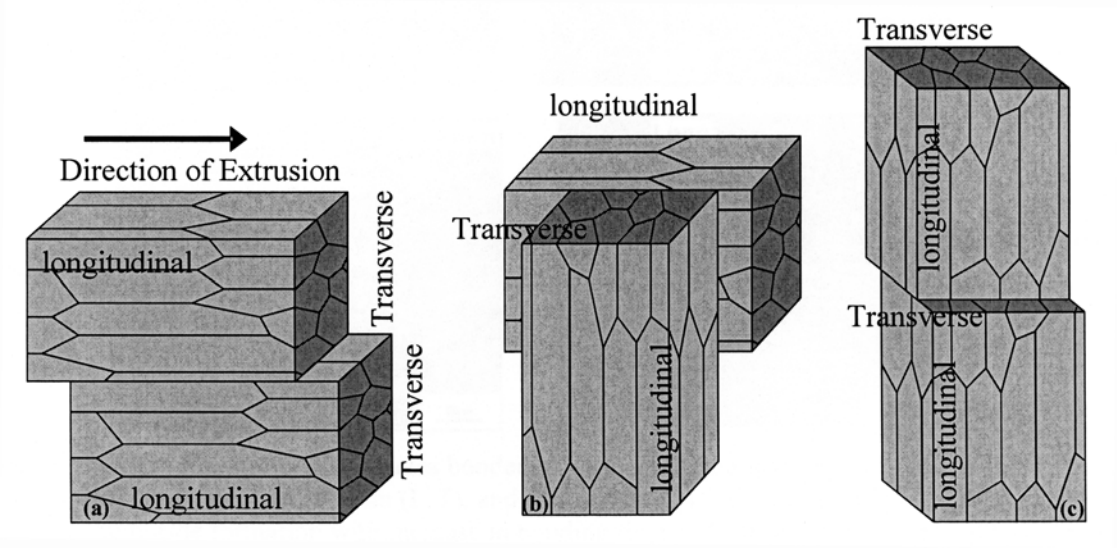

Fig. 35. Bond geometries investigated (after V. G. Krishnardula et al.[31])

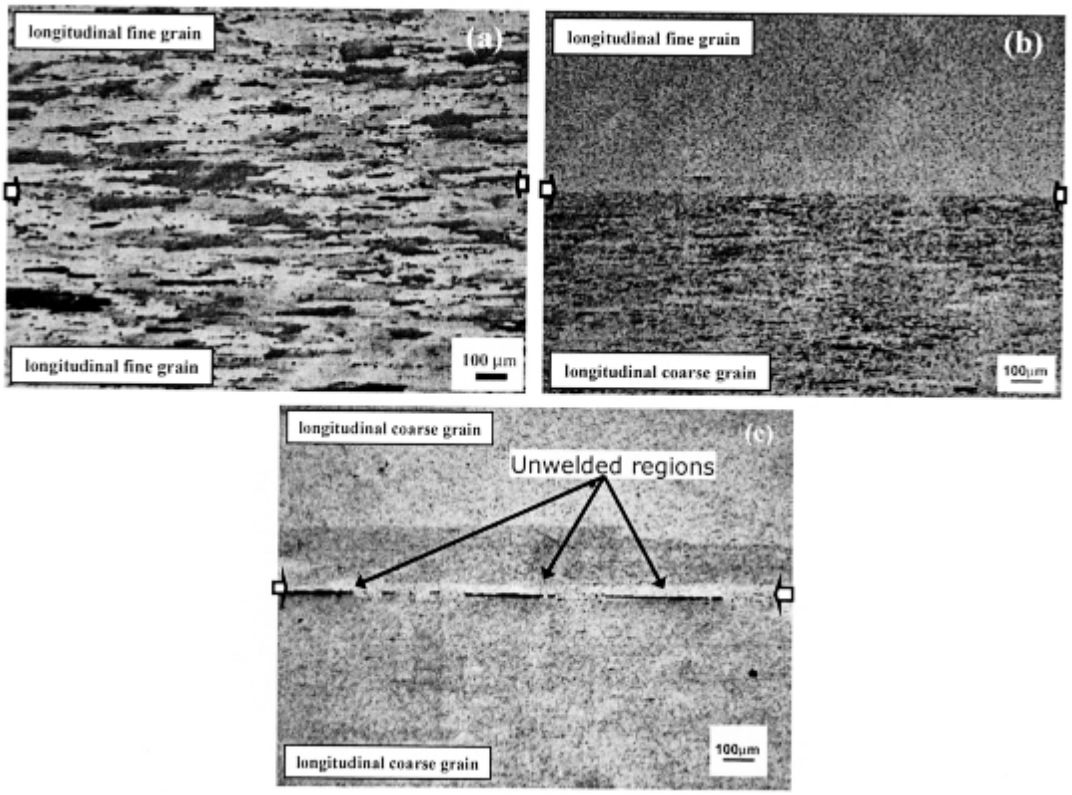

Fig. 36. Diffusion bonds in MA956 (longitudinal-longitudinal orientations, 1250°C, PBHT 1 h at 1300°C): (a) fine grain to fine grain, 121 sec; (b) fine grain to coarse grain, 170 sec; and (c) coarse grain to coarse grain, 174 sec) (after V. G. Krishnardula et al.[31]).

The unrecrystallized PM2000 also was diffusion bonded at 1250°C for up 10 min. in the longitudinal-longitudinal and transverse-transverse orientations, and bonds were formed in both cases. The best joints (in which essentially 100% of the surface was bonded), were obtained with relatively low applied stresses (1-5 MPa). Some void formation was observed in the transverse-transverse orientation, but this decreased with increasing bonding time. The PBHT resulted in recrystallization of the alloy (the authors did not indicate whether the recrystallized grains grew through the bond line), but also the formation of porosity, presumably due to gas released from the alloy. This was particularly noticeable along the bond line. Chen and Jones[42] found that such porosity could be reduced, but not eliminated, by a two-step heat treatment involving prolonged annealing at a lower temperature before the standard secondary-recrystallization treatment (1 h at 1380°C).

The results of room-temperature shear testing of PM2000 diffusion bonded in both transverse-transverse and longitudinal-longitudinal orientations followed by a PBHT of 2 h at 1385°C are compared in Fig. 37. The shear strengths of bonds in both orientations were of the order of 70% of that of the bulk, recrystallized alloy. The failures occurred at the bond lines, mostly by planar shear fracture, with some secondary cracking.

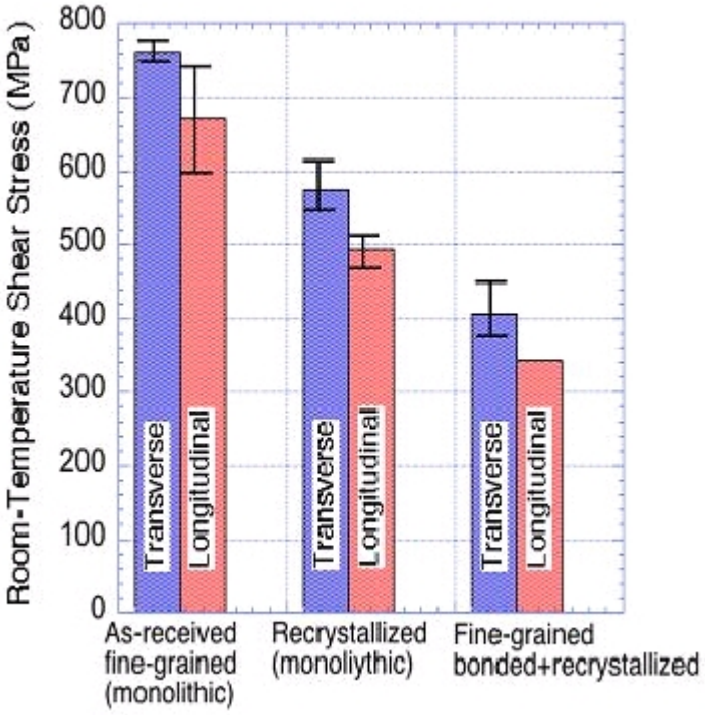

Fig. 37. Comparison of the peak room-temperature shear stresses of diffusion-bonded PM2000 (after V. G. Krishnardula, et al.[31]).

13. TRANSIENT LIQUID-PHASE BONDING

13.1 PROCESS DESCRIPTION

The transient liquid-phase (TLP) diffusion-bonding process is based on the formation between the two pieces being joined of a thin liquid layer at the bonding temperature, which subsequently solidifies to form a high-integrity joint. The parts to be joined and a thin interlayer of the TLP alloy are brought into intimate contact (excessive contact pressure is not required), and heated to a temperature above the liquidus temperature of the TLP alloy (but below the solidus temperature of the alloy being bonded). The molten phase promotes rapid local diffusion between the surfaces being bonded and, simultaneously, the principal component of the TLP alloy that most strongly influences its liquation temperature diffuses into the matrix. The loss of this element raises the melting point in the region of the liquid phase, so that the region of the bond solidifies. Because the alloys being bonded typically are designed to form a protective surface film of oxide, one function of the TLP phase is to inhibit such scale formation along the surfaces to be bonded.

13.2 APPLICATION TO ODS ALLOYS

Harper[48] reported the successful TLP bonding of ODS alloys. The joining of non-recrystallised to recrystallised material was conducted in order to cause grain growth across the interface during the joining process. The test showed that the joints appeared to be void-free with few residual particles.

Khan and Wallach[52,53,54] used interlayer foils of Fe-13% B-9% Si (wt%) for TLP bonding of MA956 and PM2000, and found that these resulted in a discontinuity in the microstructure of the parent alloy on each side of the bond line, which resulted in a weak joint. It was also not possible to induce secondary recrystallization across the bond region, apparently due to the presence of particles or a layer of oxide. However, when a sufficiently thin coating of the Fe-B-Si alloy was applied by sputtering to the surfaces to be bonded, grain growth across the TLP joint was observed after a secondary recrystallization treatment for alloy MA956, but not for PM2000.

Nakao et al.[55] also reported that joints with good creep rupture properties could be obtained via TLP bonding using an interlayer of the MA956 alloy composition modified with 7 wt% Si and 1 wt% B. The bonding conditions involved heating at 1290°C (essentially the secondary recrystallization temperature of MA956) at an applied pressure of 7 MPa, with a hold time of 0.6 hr.

Ekrami et al. also reported the ability to grow the alloy grains through the bond line during secondary recrystallization of Ni-based ODS alloy MA758 bonded using a TLP of an amorphous Ni-Cr-B-Si-based alloy.[56,57]

In a study in support of the US DOE's Generation IV Gas Fast Reactor program, researchers at Auburn University investigated the TLP bonding of MA956 (fine-grained and recrystallized) and PM2000 (fine grained).[31,52,58,59,60] The interlayer used was pure B, chosen because of its high diffusion rate in ferritic steels (no data specific to ODS alloys). The Fe-B eutectic temperature is 1174°C, and the eventual aim was to deposit interlayers of FeSiB alloys using electron beam physical deposition (EBPVD). The same equipment was used for bonding as that described earlier for diffusion bonding, the rapid heating provided by the Gleeble equipment minimizing B loss to the substrates. Mating surfaces were ground to ensure that

they were flat and parallel. Also, bonding was attempted using several orientations of the blocks to be joined (as shown earlier in Fig. 35).

The bonding parameters investigated are shown in Table 18. At a nominal bonding temperature of 1100°C, increasing the bonding time from 20 s to 1 h decreased the number of borides formed at the center-line of the bond (presumably because of diffusion of B away from the bond), but did not prevent borides forming in the substrates. No substrate recrystallization was observed in the as-bonded samples. A PBHT at 1350°C for 1 h removed all signs of borides, but did not lead to complete recrystallization of the alloy; in contrast, recrystallization of bulk MA956 is usually complete after 1 h at 1300°C. It was found that PBHT for up to 8 h at 1300°C was required to recrystallize the bonded samples.

Table 18. TLP bonding processing parameters[60]

Alloy	Initial Cndtn	Bonding parameters						PBHT	
		Interlayer	Pressure	Bond-line orientation	Heating method	Approx T	Time	T	Time
			MPa			°C	s	°C	hr
MA956	FG	1μm B	1-3	L-L parallel	Gleeble	1100	20,300, 1800,3600	1300	1
				L-L parallel	Gleeble	1250	20-3600	1300	148
				L-L cross	Gleeble	1250	20-3600	1300	
				T-T end	Gleeble	1250	20-3600	1300	8+
MA956	FG	25 μm FeSiB	5	T-T end	Gleeble	1190	150	1300	1
PM2000	FG	1μm B	1-3	L-L parallel	Gleeble	1250	30,60, 500	1385	8
			1-3	T-T end	Gleeble	1250		1385	
			<<1	L-L parallel	Furnace	1250	3600	1385	
			<<1	T-T end	Furnace	1250	3600	1385	

The microstructure shown in Fig. 38 of a bond made in fine-grained MA956 (LL parallel orientation) at 1250°C with a 1 μm B interlayer, followed by an 8 h, 1300°C PBHT illustrates the retention of some small grains at the bond-line; this feature varied markedly along the bond. The dark-appearing features along the bond line apparently were holes left by pull-out of oxide clusters during polishing. The oxide remaining in such clusters was found to be agglomerated yttria plus some alumina.

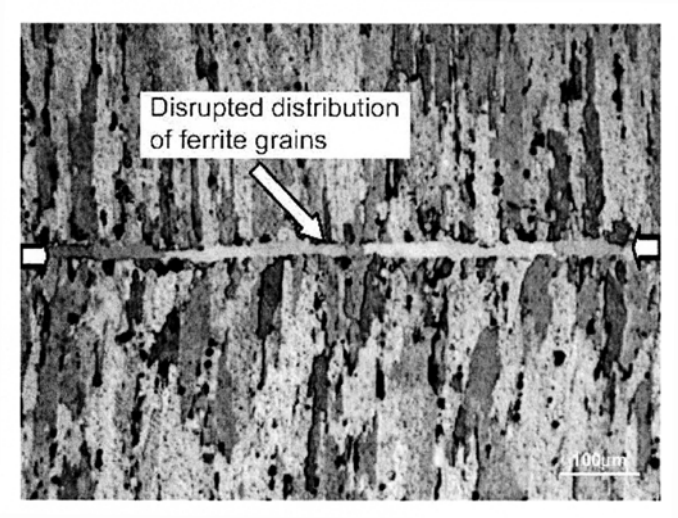

Fig. 38. Microstructure of as-PBHT specimen of MA956 (after V. G. Krishardula, et al.[60]).

An interesting phenomenon was the interaction between orientations of the recrystallized grains when the crystal orientations of the samples to be bonded were dissimilar, [i.e., orientations L-L cross, and L-T (Fig. 35)]. The best results in terms of uniformity of the final microstructure were obtained for the L-L parallel orientation. An important consideration was the thickness of the molten region present during bonding,[60] since this would be expected to disrupt the yttria particles/stringers in the affected region (leading to agglomeration), and also possibly lead to the formation of alumina particles (by interaction with Al in the alloy with oxygen in the molten phase). Since the yttria particles/stringers effectively constrain the direction in which recrystallization can occur, it would be expected that the grain size and orientation near the bond line after post-bonding recrystallization would be highly dependent on the extent of such disruption.

Processing using a 25 μm-thick interlayer of Fe-16B-5Si (weight percent) produced a well-wetted joint containing few borides, but there was a discontinuity in the recrystallized microstructure after PBHT, and the bond line remained distinct. Presumably, the relatively large amount of liquid phase caused significant disruption of the yttria dispersion, removing the constraints on the direction of recrystallization.

Baseline creep data for PM2000 are shown in Table 19. The specimens of originally fine-grained alloy were subjected to recrystallization at 1385°C for 4 h, which resulted in a coarse grain size.

Table 19. Creep rupture data for bulk PM2000 (fine grained + 1385°C for 4 h) (after Y. Chen et al.[61])

Creep rupture testing		
T, °C	**Stress, MPa**	**Life, hr**
1000	13	>185
1000	85	≈0

14. PULSED PLASMA-ASSISTED SINTERING/DIFFUSION BONDING

14.1 PROCESS DESCRIPTION

Pulsed plasma-assisted sintering or diffusion bonding, also known as pulsed electric current sintering, involves a combination of hot pressing and a pulsed (on-off) direct electric current applied to the interface to be joined through the pins that are used to transfer pressure to the sample. The process originally was developed for sintering of powders, which involves:[62]

(a) Heating of the powder by Joule heating, heat conduction from the die, and/or spark discharge between the particles.
(b) Removal of oxide films and contamination from the surfaces of the powder particles by spark discharge between the particles.
(c) Rapid heating and consolidation.

Advantages claimed are that powders can be consolidated at temperatures some 200-500°C lower than conventional sintering techniques, and in shorter times (5-20 min). In addition, grain growth and thermal damage are suppressed by the rapid heating and consolidation.

14.2 APPLICATION TO ODS ALLOYS

Nishimoto et al.[63] reported the use of this technique to join rods of recrystallized (large-grained) MA754 and MA956 by sintering with powder (of the same chemical composition as the alloys) that was inserted between the parts to be bonded. The amount of powder used was such that the thickness of the resulting bond was 0.5 to 1.0 mm. A set of graphite dies was used to hold the samples in a vacuum hot-pressing unit; processing involved a pressure of 40-70 MPa for up to 64.8 ks at 750-1142°C in a vacuum of 9.3 MPa. The bonding temperature was measured using thermocouples that contacted the surface of the sample. Densification of the bonding layer progressed rapidly in the early stages of bonding, and most of the porosity had disappeared after 360s. Densification increased rapidly with increasing bonding temperature, with increasing bonding pressure, and was slightly accelerated with smaller powder particles sizes (65 μm compared to 240 μm).

TEM examination indicated no evidence of melting at the interfaces between the particles and the samples being bonded, so that the density of the dispersion and size of the yttria particles in the bond was comparable to those in the monolithic alloy. Unfortunately, no metallographic information was provided on the microstructure of the bond, or of that of the joined parts in the vicinity of the bond.

Creep testing in air at 650°C and 88-250 MPa was conducted using specimens bonded at 1050°C (MA956) and 1100°C (MA754). Creep rupture lives were found to increase with increasing hold time during bonding, as shown in Fig. 39, attaining approximately 70% of the strength of the respective base alloys in the axial direction. Fig. 40 indicates that the axial creep-rupture strengths of large-grained MA754 and 956 were consistently higher than those of samples bonded by friction welding, TLP diffusion bonding, or solid-state diffusion bonding, and quite close to those of the monolithic materials.

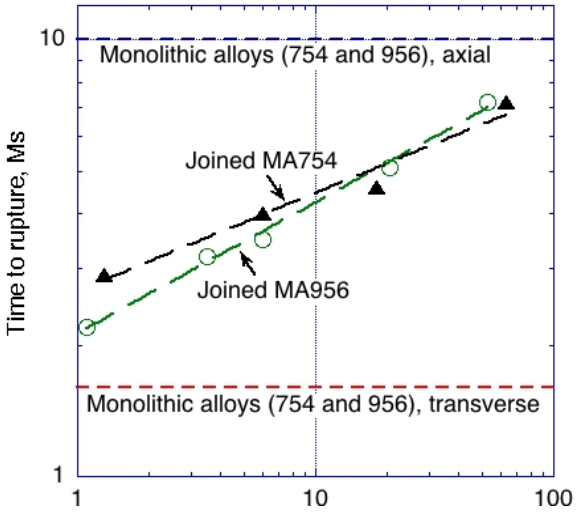

Fig. 39. Effect of holding time on creep-rupture life of large-grained MA754 and MA956 joined by pulsed plasma-assisted bonding (after Nishimoto et al.[63]).

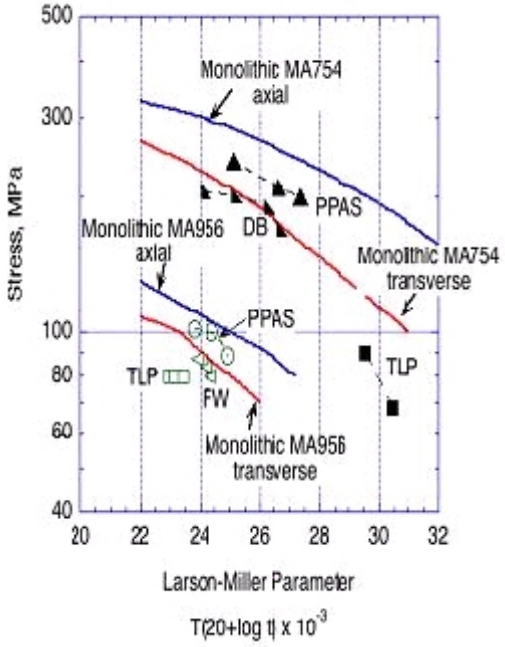

Fig. 40. Comparison of creep-rupture strength of large-grained MA754 and MA956 joined by different techniques: PPAS-pulsed plasma-assisted sintering; DB-diffusion bonding; TLP-transient liquid-phase bonding; FW-friction welding (after Nishimoto et al.[63]).

The Materials and Electrochemical Research (MER) Corp., Tucson, AZ demonstrated the use of pulsed plasma-assisted diffusion bonding to make direct butt joints in PM2000 without the need for filler powder.[64] Figure 41(a) shows schematically the pulse-sintering press design initially used for unsupported samples. The advantage of this scheme is that, since the specimens are not contained in a die, it is possible to measure their temperatures directly during bonding. A major drawback encountered was the pressure that can be applied was limited because, at the joining temperature (1100°C), the ductility of the alloys led to significant plastic deformation if excessive pressure was applied, the bonded part lost its shape, and the microstructure at the joint deteriorated. Figure 41(b) shows a modification of the press to allow the application of high pressure during bonding, in which the parts being bonded are encapsulated in a high-temperature graphite die. One problem with this configuration is that it is impossible to measure the sample temperature directly, since the provision of any penetrating hole in the die (either for a thermocouple, or for a pyrometer) is precluded due to the high pressure applied.

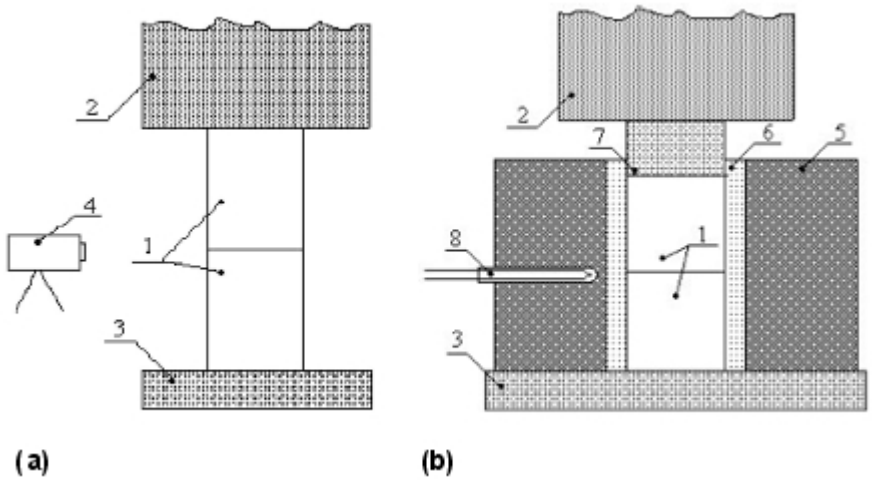

Fig. 41. Schematic diagram of MER's rig for plasma-assisted joining (a) of unsupported work pieces; and (b) of supported work pieces (after E. Dyadko et al.[64]). (1 – pieces to be bonded; 2 – ram; 3 – base; 4 – pyrometer; 5 – die; 6 – insulation; 7 – pin; 8 – thermocouple).

Initial attempts at bonding used samples of fully-recrystallized MA956. Later work used 19 mm diameter rods of unrecrystallized MA956 from a US DOE project conducted by Special Metals Corp. and the Edison Welding Institute.[30] The thermal history of the rod samples used for joining is shown in Table 20. The samples to be bonded were polished on a lapping machine using SiC sandpaper up to 1200 grit (U.S.), ultrasonically cleaned sequentially in acetone and ethanol, and assembled in the pulse-sintering machine. In order to control plastic deformation of the samples during joining, an indicator was installed on the pulse-sintering machine to enable downward movement of the ram to be measured, thus allowing the pressure applied to be corrected before sample distortion became severe.

Because of the difference in high-temperature creep behavior of unrecrystallized (approx. 1 μm grain size) and fully recrystallized MA956 (very large, elongated grains), initial testing was conducted to allow appropriate adjustment of the bonding parameters. Bonding was carried out in an Ar atmosphere at 9V, 1000A, 62Hz, 70% duty cycle. Table 20 lists the change in specimen dimensions after joining.

Table 20. Properties of Incoloy MA956 blanks used for joining[64]

Sample #	Batch #	Extrusion ratio	Extrusion temperature °C	Annealing temperature °C	Anneal time hr	Diameter mm	Length, mm		
							Before joining	After joining	D mm (%)
MA-21	A1A1A1	10 : 1	1000	1000	0.5	19.1	25.0	44.9	5.2 (10.4)
	A1A1A2	10 : 1	1000	1000	1.0	19.2	25.1		
MA-23	A1A1A3	10 : 1	1000	1000	6.0	19.4	25.0	47.7	2.7 (5.4)
	A1B1A3	10 : 1	1075	1000	6.0	19.1	25.4		
MA-22	A1B1A1	10 : 1	1075	1000	0.5	19.2	24.1	47.0	1.2 (2.5)
	A1B1A2	10 : 1	1075	1000	1.0	19.3	24.1		
MA-26	A1C1A3	10 : 1	1150	1000	6.0	18.7	24.2	47.8	0.6 (1.2)
	A1D1A3	10 : 1	1200	1000	6.0	19.2	24.2		
MA-24	A1C1A1	10 : 1	1150	1000	0.5	19.0	25.0	48.5	1.5 (3.0)
	A1C1A2	10 : 1	1150	100	1.0	19.1	25.0		
MA-25	A1D1A1	10 : 1	1200	1000	0.5	19.1	24.6	47.6	1.5 (3.1)
	A1D1A2	10 : 1	1200	1000	1.0	19.1	24.5		

Figure 42 indicates that some samples after joining lost their shapes and changed lengths, as a result of an inappropriate combination of processing temperature and pressure.

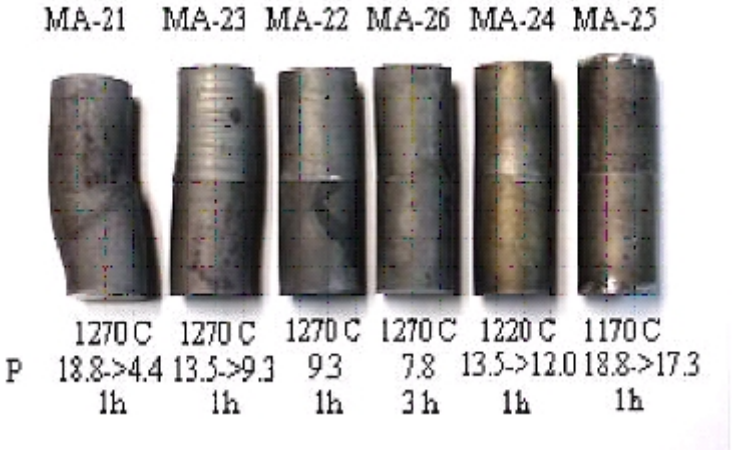

Fig. 42. Appearance of samples after joining (after E. Dyadko et al.[64]).

The dependence of a change in length on the maximum pressure applied was close to linear (Fig. 43). The experimental results showed that at 1270°C even at the low pressure 7.8 MPa slight creep occurred (Specimen MA-26). Initial application of excessive pressure dramatically increased the creep rate, even if the pressure was significantly decreased after a short time. Thus, during run MA-22, a pressure of 9.3 MPa for 60 min caused only a 2.5% decrease in length, whereas during run MA-21, initial application of a pressure of 18.8 MPa, rapidly reduced to 9.3 MPa, resulted in the same creep after only one minute. This behavior illustrates the necessity of a detailed knowledge of the mechanical behavior of the specific form of alloy being processed. After cooling from bonding temperature, the bonded rods were machined by EDM to prepare bar samples ~5 cm long for cold flexural strength and high-temperature creep rate testing. The samples were extracted as shown in Fig. 44.

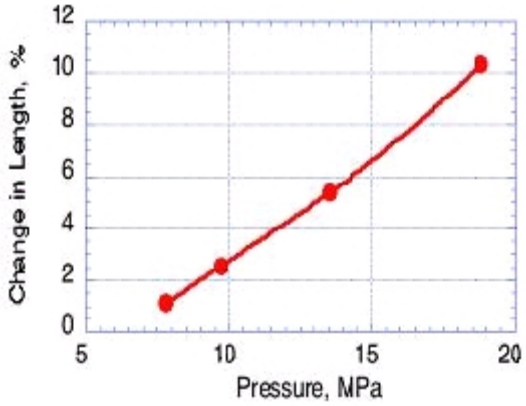

Fig. 43. Dependence of change in length of sample after bonding on maximum applied pressure (after E. Dyadko et al.[64]).

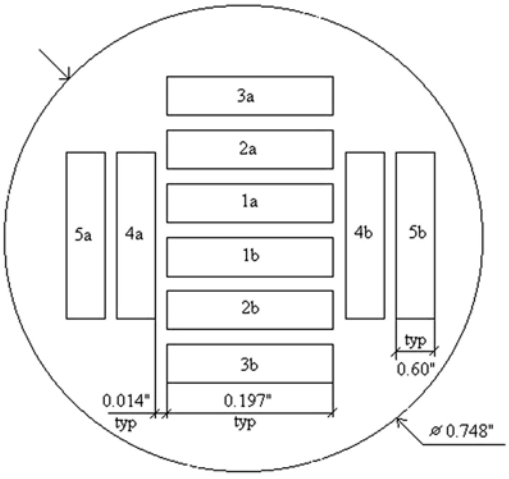

Fig. 44. EDM cutting scheme (after E. Dyadko et al.[64]).

Cold flexural testing was carried out by four-point bending (17 mm upper span, 36 mm lower span). The typical loading diagram is shown in Fig. 45, and the results are presented in Table 21.

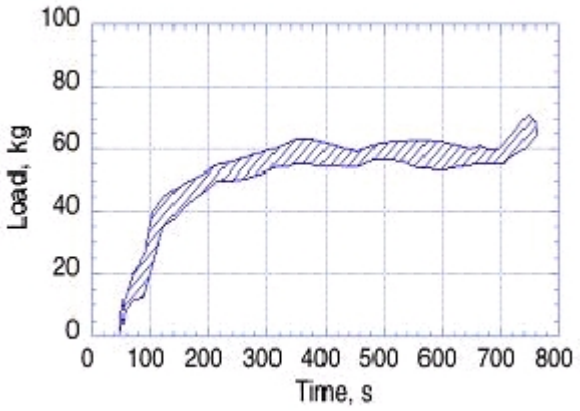

Fig. 45. Cold flexural testing result for sample MA-24 (after E. Dyadko et al.[64]).

Table 21. Cold flexural strength testing results[64]

Specimen #	Bonding parameters			Max load, MPa	Result
	T°C	P, MPa	Hold time, h		
MA-21	1270	18.8 to 4.4	1	23	rupture
MA-23	1270	13.5 to 9.3	1	80	no rupture
MA-22	1270	9.3	1	80	no rupture
MA-26	1270	7.8	3	76	no rupture
MA-24	1220	13.5 to 12.0	1	91	no rupture
MA-25	1170	18.8 to 17.3	1	78	rupture

Sample MA-21 that was bonded at 1270°C and maximum pressure showed the smallest strength, and broke at the bonding interface (Fig. 46). Sample MA-25, bonded at 1170°C and maximum pressure, also broke at the interface, but at significantly higher stress. All the other samples did not break, but bent uniformly at approximately the same stress until their medium points touched the bottom fixture, indicating that the strength of the joints were not less than that of the bulk material. It is of note that in all cases the maximum stress was low, but this is a property of the bulk, unrecrystallized alloy, rather than being due to the joints. For comparison one sample was bonded by hot pressing without plasma assistance at 1270°C, 60 MPa, 1 h in a vacuum atmosphere in a graphite die. Joining did not occur and the sample fell apart during EDM cutting.

Fig. 46. Macro views of samples after cold flexural testing (after E. Dyadko et al.[64]).

This joining technique is the subject of a continuing collaboration between MER Corp. and the Oak Ridge National Laboratory, in which evaluation of creep strength at 1000°C and correlation with the microstructures of the joints are being used to provide guidance for optimizing the process parameters.[2,64] The extent to which this technique can produce joints which approach the idealized microstructure can be gauged by the fact that the load to cause failure of PM2000 in the creep tests has been measured to be in excess of 82% of that to fail the monolithic alloy.[2,64,65]

15. MECHANICAL JOINTS

15.1 PROCESS DESCRIPTION

Where there is no requirement to provide the function of a pressure boundary, there are several options available for the mechanical joining of ODS alloys that also would function at the high service temperatures typically involved. Explosive bonding and pulsed magnetic welding arguably could be classified as mechanical joining processes, but these technologies were described separately in Sections 9 and 11, respectively. Particular examples of relatively small components of ODS alloys that rely on mechanical joining are airfoils in gas turbine engines, where a system of mechanical interlocking is used. Simple bolting of components also can be effective, and the use of threaded joints with a seal weld could conceivably withstand some level of pressure differential. Such relatively straightforward approaches often are overlooked where 'advanced' technologies are employed, but have the potential for providing an adequate solution.

15.2 APPLICATION TO ODS ALLOYS

Roll welding of ribbed panels of TD-NiCr was proposed for the fabrication of heat shields for the space shuttle [Holko et al.[7]]. The vertical ribs were 0.25 mm tall, and the face sheet was 0.3 mm thick. While the best joints were made at 980°C using three roll passes at 20% reduction per pass, some degree of rib cracking was observed, an the microstructure at the rib-face sheet developed a fine grain size.

A sample of alloy PM2000 was applied as an uncooled plate component in the area of the upper air nozzles of the Mussalo coal-fired power plant of Pohjolan Voima in Kotka, Finland, under service conditions where the original material selection (Sandvik MA253: Fe-21Cr-11Ni-1.7Si-N-Ce) had experienced serious oxidation and deformation problems after six months of service (Fig. 47).[22] All the necessary joining was done by mechanical locking to an MA253 frame. The service temperature of the nozzle was estimated to lie in the range 900-1000°C. In this test, the central uncooled plate section of the end nozzle was replaced with PM2000. After about one year of plant testing, no visible warping was observed of the PM2000 component, and within the measuring accuracy of about ±0.05 mm), no wall thinning was observed on any location of the component, including the edges directly facing fireside radiation from the boiler.

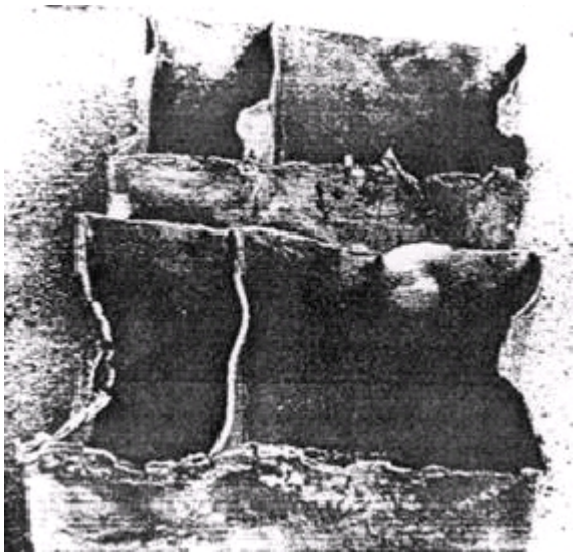

Fig. 47. Original nozzles (Sandvik MA253) after six months of service. (After S. Holmstrom et al. [22]).

16. OVERALL CONCLUSIONS

There are clearly several techniques available for joining ODS alloys. Notably, while the fusion welding processes typically employed with wrought alloys produce the least satisfactory results with ODS alloys, some versions, such as fusion spot welding and the laser and electron-beam welding technologies, have been demonstrated to have the potential for producing sound joints. Welds made using solid-state spot welding reportedly have exhibited parent metal properties.

The overall goal for optimum joining of ODS alloys is a joint with no local disruption of the distribution of the oxide dispersion, and no significant change in the size and orientation of the alloy microstructure. The techniques that come closest to this ideal involve solid-state diffusion bonding and, in particular, it has been found secondary recrystallization of joints made by pulsed plasma-assisted diffusion can produce the desired, continuous, large alloy grain structure through the joint. Such joints have exhibited creep rupture failure at >82% of the load needed to fail the monolithic parent alloy at 1000°C.

In addition, there is a range of joining techniques capable of serious application to ODS alloys, even though they result in disruption of the alloy microstructure. The key to the use of such techniques is adjustment of the processing parameters to minimize the extent of or influence of the changes in the alloy microstructure. Selection among these joining approaches largely depends on the particular application and component configuration, and an understanding of the relationships among processing, alloy microstructure, and final properties. Examination of such techniques historically has been driven by two principal applications: joining sheet, such as for heat shield applications (originally for the skin for the US space shuttle), and joining of tubes for fuel pins in nuclear breeder reactors and for high-temperature heat exchangers. Prime examples of the latter are the successful construction and demonstration using explosively-bonded or brazed joints in heat exchangers for heating air to 1000°C. The differences in the forms of the alloys used for these applications have resulted in different considerations for the joining techniques, each of which has its own peculiar requirements for surface preparation, tooling and fixturing. Recent developments have resulted in friction welding evolving to be a prime method for joining ODS sheet products, and variants of diffusion bonding and brazing have shown excellent promise for use with tubes and pipes.

The intention of this report is to provide a consolidated source of information on all joining techniques that have been attempted for ODS alloys, to facilitate the choice of potential techniques for any component configuration considered. While care has been taken to include all available information reported that is pertinent to choosing among techniques, perusal of the original data sources is recommended. Where the next step to joining trials is taken, detailed examination of the as-joined and post-test microstructures is strongly urged to provide a rational basis for evaluating the results, rather than simple reliance on accurate control of the processing parameters. Such observations also could lead to the selection of appropriate methods for the non-destructive evaluation of such joints. Because there are, as yet, few reported instances of the use of joined ODS structures in commercial service, it is important to begin the development of a database of practical experience.

REFERENCES

1. L. E. Shoemaker, "Joining techniques for a ferritic oxide dispersion-strengthened alloy," pp. 371-377 in *Advances in Welding Science and Technology*, S. A. David, Ed., ASM International (1986).

2. See, for instance, I. G. Wright, B. A. Pint, E. G. Dyadko, N. S. Bornstein, and G. J. Tatlock, "Enabling the Practical Application of Oxide Dispersion-Strengthened Ferritic Steels," *Proc. 21st Annual Conference on Fossil Energy Materials*, Knoxville, Tennessee, April 30-May 2, 2007.

3. See, for instance, B. K. Kad, I. G. Wright, and R. R. Judkins, "Solid-State Joining Oxide Dispersion Strengthened Alloy Tubes," *Proc. 21st Annual Conference on Fossil Energy Materials*, Knoxville, Tennessee, April 30-May 2, 2007.

4. See, for instance, G. J. Tatlock, H. Al-Badairy, C-L. Chen, A. R. Jones, "Control of Defects and Microstructure in ODS Alloys," *Proc. 21st Annual Conference on Fossil Energy Materials*, Knoxville, Tennessee, April 30-May 2, 2007.

5. Data source: "2000 Matter," University of Liverpool, UK (2000). www.matter.org.uk/steelmatter/manufacturing/welding/fusion.html.

6. *Special Metals Corp. Technical Bulletin on Incoloy MA 956*, Publication Number SMC-008 (2004).

7. K. H. Holko, T.J. Moore, and C. A. Gyorgak, "State-of-technology for joining TD-NiCr sheet," NASA TM X-68070 (1972).

8. T. J. Kelly, pp. 215-220 in *Proc. Symp. on Laser-Solid Interactions and Laser Processing*, Boston, Materials Research Society (1978).

9. Private communication, Gaylord Smith, Special Metals Corp., Huntington, West Virginia, 2005.

10. M. L. Hamilton, D. S. Gelles, R. J. Lobsinger, G. D. Johnson, W. F. Brown, M. M. Paxton, R. J. Puigh, C. R. Eiholzer, C. Martin, and M. A. Blotter, pp. 38-39 in *Fabrication Technological Development of the Oxide Dispersion-Strengthened Alloy MA957 for Fast Reactor Applications*, Report No. PNNL-13168, Feb. 2000.

11. P. Molian, Y. M. Yang, and P. C. Patnaik, *J. Mater. Sci.*, 27, 2687 (1992).

12. W. D. Klopp, Section FeNM-1450 (MA956) on Ferritic Stainless Steels, *Aerospace Structural Metals Handbook* (1992).

13. M.G. McKimpson and D. O'Donnell, "Joining ODS Materials for high-temperature applications," *JOM*, 46 (7), 49-51 (1994).

14. H.D. Hedrich, H.G. Meyer, G. Haufler, M. Kopf, and N. Reheis, “Joining of ODS superalloys,” pp. 789-798 in *High-Temperature Materials for Power Engineering 1990, Part I, E*, Bachelet et al., Eds., Kluwer Academic Publishers (1990).

15. C. Brown, E. Verghese, D. Sporer, and R. Sellors, “PM2000 honeycomb structures,” paper No. 98-GT-565, presented at the *43rd ASME Gas Turbine and Aeroengine Technical Congress*, Stockholm, Sweden, 1998.

16. *Practical Welding Letter* No. 024 August 01, 2005.

17. “Introduction to Furnace Brazing,” Air Products and Chemicals, Inc., Allentown, PA (2001).

18. D. O’Donnell, “Joining of oxide dispersion-strengthened materials,” pp. 1037-1040 in *ASM Handbook Vol. 6: Welding, Brazing, and Soldering*, ASM International, Materials Park, Ohio (1993).

19. T.J. Kelly, “Brazing of Inconel Alloy MA754 for high-temperature applications,” *Welding J.*, 61 (10), 317-319 (1982).

20. D.J. Seery and J. Sangiovanni, “Engineering development of a coal-fired high-performance power generating system,” Paper No. 1.7 in *Proc. of the Advanced Coal-Based Power and Environmental Systems’98 Conference*, Morgantown, West Virginia, July 21-23, 1998, DOE/FETC-98/1072.

21. Private communication, N.S. Bornstein and D.J. Seery, United Technologies Research Center, Middletown, Connecticut.

22. S. Holmstrom, M. Siren, L. Heikinheimo, P. Auerkari, J. Varmavuo, and R. Saarinen, “Performance of an iron-based ODS Alloy in a boiler environment,” pp. 769-777 in *Materials for Advanced Power Engineering 1998*, LeComte-Beckers, F. Schubert, and P. J. Ennis, Eds., Forschungszentrum, Zentralbibliothek, 1998.

23. F. Olsson, S. A. Svensson, and R. Duncan, “Externally-fired gas turbine cycles with high-temperature heat exchangers utilizing Fe-based alloy tubing,” pp. 139-153 in *Proc. 15th Plansee Seminar, G. Kneringer*, P. Rodhammer, and H. Wildner, Eds., Plansee Holding AG., Reutte (2001).

24. B. Tabernig, W. Thierfelder, H. Alber, and K. Sudmeijer, “Fabrication of metallic honeycomb panels for reusable TPS structures,” Paper No. RM 90, pp. 746-760 in *Vol. 1 of Proc. 15th Intl. Plansee Seminar*, G. Kneringer, P. Rödhammer, and H. Wildner, Eds., Plansee Holding AG, Reutte, Austria (2001).

25. J. Price, “Advanced Materials for Mercury 50 Gas Turbine Combustion System,” presented at the *U.S. Department of Energy Distributed Energy Peer Review*, Arlington, VA, Dec 200518.

26. The Welding Processes: Resistance Welding," *Key to Steel Database, Key to Steel North America*, St. Louis, MO; www.key-to-steel.com.

27. S. de Burbure de Wesembeek, "Resistance butt welding of dispersion-hardened ferritic steels," *Proc. 3rd Intl. Conf. on Advances in Welding Processes*, Harrogate, May 7-9, 1974.

28. L. DeWilde, J. Gedopt, S. De Burbyre, and A. Delbrassine, "Pilot-scale fabrication of ODS-ferritic alloy components for fast-breeder reactor fuel pins," Paper No. 50 in *Matls. For Nuclear Reactor Core Applications*, BNES, London (1987).J. Bottcher, S. Ukai, and M. Inoue, *Welding J.*, 138, 238 (2002).

29. J. Bottcher, S. Ukai, and M. Inoue, *Welding J.*, 138, 238 (2002).

30. See, for instance, L. E. Brown, B. K. Kad, G. Smith, A. Robertson, and I. G. Wright, *Development of ODS Heat Exchanger Tubing*, Final Technical Report on EWI Project No. 47572GTH on DOE Contracts DE-C26-00NT40970 and DE-FC26-05NT42238 (2008).

31. V. G. Krishnardula, D. E. Clark, and T. C. Totemeier, *Joining Techniques for Ferritic ODS Alloys*, Report No. INL/EXT-05-00385 on US DOE Office of Nuclear Energy Contract No. DE-AC07-051D14517, June 2005.

32. W. F. Brown, J. Bandas, and N. T. Olson, "Pulsed magnetic welding of breeder reactor fuel pin end enclosures," presented at the AWS 59th Annual Meeting, New Orleans, Louisiana (1978).

33. T. I. Kahn and E. R Wallach, *Mater, Sci. Techn.*, 12, 603 (1996).

34. P. Miao, G. R. Odette, J. Gould, J. Bernath, R. Miller, M. Alinger, and C. Zanis, "The microstructure and strength properties of MA957 nanostructured ferritic alloy joints produced by friction-stir and electro-spark deposition welding," *J. Nucl. Mat.*, 367-370, 1197-1202 (2007).

35. B. Crossland, *Explosive Welding of Metals and its Application*, Oxford University Press (1982).

36. P. W. Jackson, N. P. Marsh, G.A.J. Hack, and M.J . Shaw, "Explosive welding of ODS Inconel MA956," *Welding and Metal Fabrication*, 58 (2), 84-92 (1990).

37. F. Starr, A. R. White, and B. Kazimierzak, pp. 1393-1412 in *Materials for Advanced Power Engineering 1994*, D. Coutsouradis, et al., Eds., (Kluwer Academic Publishers, 1994).

38. *The British Gas Closed Cycle Demonstrator*, British Gas, Final Year Report (1995).

39. See, for instance, S. Kallee and D. Nicholas, "Friction Stir Welding at TWI," TWI Information 2004; www.twi.co.uk.

40. W. M Thomas, E. D. Nicholas, J. C Needham, M. G. Murch, P. Templesmith, C. J. Dawes, International Patent Application N. British Patent Application No. 9125978.8 (1991).

41. A. Bucklow, S. B. Dunkerton and P. L. Threadgill, The Welding Institute, Cambridge, UK, TWI Members report 570 (1996).

42. L. E. Murr, G. Liu and J. C. McClure, *J. Mater. Sci.*, 33, 1243 (1998).

43. C. Capdevila and H.K.D.H. Bhadeshia, "Manufacturing and microstructural evolution of mechanically-alloyed oxide dispersion-strengthened superalloys," *Advanced Engineering Materials*, 3 (9), 647-656 (2001).

44. K. Shinosaki, American Welding Society, pp289-299, August 1997.

45. K. Shinozaki, C. Y. Kang, Y. C. Kim, M. Aritoshi, T. H. North, and Y. Nakao, "The Metallurgical and Mechanical properties of ODS alloy MA956 friction welds," *Welding Journal*, 76 (8), 289-299, (1997).

46. P. L. Threadgill, *Friction Welding of an Fe_3Al-based ODS Alloy*, Report No. ORNL/Sub/97-SX373/01, July 1998.

47. K. Shinosaki, American Welding Society, pp289-299, August 1997.

48. K. Shinozaki, C. Y. Kang, Y. C. Kim, M. Aritoshi, T. H. North, and Y. Nakao, "The Metallurgical and Mechanical properties of ODS alloy MA956 friction welds," *Welding Journal*, 76 (8), 289-299, (1997).

49. Z. Feng and W. Ren, *Initial development in joining of ODS alloys using friction-stir welding*, Report No. ORNL/GEN4/LTR-06-021 (2006).

50. Magneform, San Diego, CA; www.magneform.com

51. T. J. Moore, T. K. Glasgow, "Diffusion welding of MA6000 and a conventional Ni-based superalloy," *Welding Journal*, 64 (8), 219-226 (1985).

52. T. I. Kahn and E. R. Wallach, *J. Mater. Sci.*, 30, 5151 (1995).

53. T. I. Kahn and E. R Wallach, "Transient liquid-phase diffusion bonding and associated recrystallization phenomenon when joining ODS ferritic superalloys," *J. Mater, Sci.*, 31 (11), 2937-2943 (1996).

54. T. I. Kahn and E. R. Wallach, Materials Science and Technology, 12, 603 (1996).

55. Y. Nakao and K. Shinosaki, Materials Science and Technology, 11, 304-311 (1995).

56. A. Ekrami and T. I. Khan, Materials Science and Technology, 15, 946-950 (1999).

57. A. Ekrami, T. I. Khan and M. Hassan, “The effect of transient liquid phase diffusion bonding on the properties of an ODS nickel alloy MA758,” *Materials Science and Technol.,* 19, 132-136 (2003).

58. W. F. Gale, “Transient Liquid Phase Bonding of Ferritic ODS Alloys,” Progress reports on U.S. DOE Office of Nuclear Energy, Idaho National Laboratory Subcontract No. 00020828, 2003-2004.

59. W. F. Gale and D. A. Butts, “Transient Liquid Phase Bonding,” *Sci. And Techn. Of Welding and Joining,* 9 (4), 283-300 (2004).

60. V. G. Krishnardula, N. I. Sofrijon W. F. Gale, and J. W. Fergus, “Transient Liquid Phase Bonding of Ferritic Oxide Bonding of Ferritic Oxide Dispersion-Strengthened Alloys,” *Met. & Mat. Trans. A*, 37, 497-500 (2006).

61. Y, L. Chen and A. R. Jones, *Met. & Mat. Trans.*, A, 36, 785 (2001).

62. M. Tokita, “Mechanism of spark plasma sintering,” pp. 69-76 in *Proc. Intl. Symp. On Microwave, Plasma, and Thermochemical Processing of Advanced Materials*, S. Miyake and M. Samandi, Eds., Elsevier (1997).

63. K. Nishimoto, K. Sida, and R. Tsuduki, “In situ sintering bonding of oxide dispersion-strengthened superalloys using pulsed electric current sintering technique,” *Sci. & Techn. of Welding & Joining*, 9 (6), 493-500 (2004).

64. E. Dyadko, *Novel Joining Technique for Oxide Dispersion-Strengthened Iron Aluminide Alloys, Quarterly report 7*, under Contract No. DE-FG03-00ER83041, by Materials and Electrochemical Research (MER) Corporation, Tucson, AZ, September, 30, 2003.

65. G. J. Tatlock, E. G. Dyadko, S. N. Dryepondt, and I. G. Wright, ”Pulsed Plasma-Assisted Diffusion Bonding of ODS-FeCrAl Alloys,” *Met. & Matls. Trans. A*, 38, 1663-1665 (2007).